PHYSICAL REVIEW B VOLUME 15, NUMBER 1 1 JANUARY 1977

Non-Arrhenius diffusional behavior and high-field nuclear spin relaxation in crystals

Dieter Wolf
*Department of Physics, University of Utah, Salt Lake City, Utah 84112**
(Received 19 April 1976)

In terms of Eisenstadt and Redfield's encounter model, the dipolar pair correlation functions associated with two point-defect mechanisms of self-diffusion in cubic crystals assumed to rearrange the nuclear spins simultaneously, are calculated. As a special case, the correlation functions for a single correlated self-diffusion mechanism presented earlier are obtained. Also, assuming random nearest-neighbor jumps of the atoms arranged in a crystal lattice, the random-walk correlation functions of Torrey, Eisenstadt and Redfield, Sholl, and the present author are included in the limit of uncorrelated self-diffusion. Starting from the Fourier-transform relations between the nuclear spin relaxation rates and the dipolar pair correlation functions, the high-field relaxation properties due to two point-defect mechanisms are analyzed in the temperature region where the related Arrhenius plot shows a curvature. For the simultaneous self-diffusion via mono- and divacancies in fcc and bcc single crystals, it is found that the orientation dependences of the high-field relaxation rates are not much affected by a change of the dominant diffusion mechanism. However, the effect of different activation energies and attempt frequencies assumed to characterize the two mechanisms results in asymmetric shapes of the T_1 and $T_{1\rho}$ minimum as a function of temperature. It is illustrated how these phenomena allow one to determine *both* self-diffusion mechanisms involved if the related T_1 and (or) $T_{1\rho}$ minimum may be studied experimentally in the temperature region where the dominant self-diffusion mechanism changes, i.e., where the corresponding Arrhenius plot exhibits a curvature.

I. INTRODUCTION

In the wide temperature range over which thermally activated self-diffusion processes in cubic crystals may be studied by means of different experimental techniques, quite frequently temperature-dependent values of the activation energy of the diffusion process are obtained from the related Arrhenius plots. This effect is usually attributed to the change of the dominant diffusion mechanism due to the different activation energies E_1 and E_2 associated with two different mechanisms.[1] Therefore, the total macroscopic self-diffusion coefficient D is assumed to be the sum of the two partial self-diffusion coefficients, D_1 and D_2:

$$D = D_1 + D_2 = D_{01} e^{-E_1/kT} + D_{02} e^{-E_2/kT}, \tag{1.1}$$

where D_{01} and D_{02} are the so-called pre-exponential factors.

Thus, e.g., by means of the radioactive-tracer method the diffusion mechanisms in the face-center cubic (fcc) metals (e.g., Cu, Ag, Au, Pb, and Al) have been identified as the single and divacancy mechanisms, using measurements of the temperature and pressure dependence of the diffusion coefficients, as well as the isotope effect.[1,2] The diffusion properties of the fcc metals may be characterized entirely by single vacancies at temperatures up to about $T \approx \frac{2}{3} T_m$ (T_m is the melting temperature), while for $T > \frac{2}{3} T_m$, divacancies may become more and more important.[3]

In body-centered cubic (bcc) metals (e.g., Li, Na, K) the curvature of the Arrhenius plot is usually even more pronounced than in the fcc metals, but the mechanisms acting there are not quite as well understood, partly because of the complexity of the possible divacancy mechanisms. (An excellent review of these and other questions is found in Ref. 3.)

A curvature of the Arrhenius plot has also been observed in ionic crystals. Thus, e.g., in CaF_2 (a material containing one nuclear spin sort only) an increase of the activation energy of self-diffusion is found from nuclear-magnetic-resonance (NMR)[4] and ionic conductivity measurements[5,6] as the temperature is increased.

A great virtue of NMR as a method to study self-diffusion in crystals lies in that (i) it is able to provide information about the *relative* motions of the nuclear spins which are known to be strongly influenced by correlations of successive jumps,[7,8] and (ii) by virtue of the time scale inherent in NMR experiments (represented by the Larmor precession frequency of the nuclear magnetic moments), the correlated jumps of atoms may be separated from the random jumps of point defects. Also, the atomic jumps induced by the *same* point defect may be distinguished from those caused by different point defects. In the radioactive-tracer method all these correlation effects are accounted for by the correlation factor f defined by

$$D^{\mathrm{tr}} = fD, \tag{1.2}$$

where D^{tr} is the tracer self-diffusion coefficient.

The comparison of diffusion constants deter-

mined from NMR experiments with those obtained with other (more direct) experimental methods is complicated by (i) the difficulties of identifying *all* sources of relaxation, and (ii) the considerable theoretical efforts necessary to relate the measured relaxation times T_1 (spin-lattice relaxation time), T_2 (spin-spin relaxation time), and $T_{1\rho}$ (spin-lattice relaxation time in the rotating frame) to the mean time τ between consecutive jumps of an atom. τ is related to the macroscopic diffusion coefficient D by the Einstein-Smoluchovsky relation

$$D = d^2/6\tau \,, \tag{1.3}$$

where d denotes the nearest-neighbor jump distance of the atoms.

Therefore, the goal of NMR in determining diffusion *mechanisms* is to detect *relative changes* of the relaxation times as a function of experimental parameters (temperature, crystallographic orientation and magnitude of the Zeeman field $\vec{H}_0$) rather than their *absolute values*. Two such effects have been found: (i) The variations of T_1, T_2, and $T_{1\rho}$ as a function of the orientation of the strong constant external field $\vec{H}_0$ with respect to the main crystal axes may be characteristic for a given diffusion mechanism.[8-10] (ii) Shape and width of the T_1 and $T_{1\rho}$ minimum as a function of temperature are functions of the type of point-defect causing the atomic motions.[8] The main problems associated with the first method are the relatively small differences predicted for different diffusion mechanisms which, in practice, allow one to distinguish correlated from uncorrelated motions, but not easily different types of correlated mechanisms.[11]

The second method may be used to study diffusion both in single crystals and in polycrystalline samples. It, therefore, seems to be rather promising in its application to metals.

As illustrated earlier,[7] the prediction of anisotropies, temperature, and field dependences of relaxation times in the motionally narrowed region may be reduced to the calculation of the Fourier transforms $J^{(q)}(\omega)$ of the dipolar pair correlation functions

$$G^{(q)}(t) = \frac{1}{N}\sum_i \sum_j \langle F_{im}^{(q)}(t') F_{im}^{(q)*}(t'+t)\rangle_{t'} , \tag{1.4}$$

for a given self-diffusion mechanism. Here, in the well-known fashion,[12] the functions $F_{im}^{(q)}(t)$ symbolize the geometrical part of the direct dipolar interaction of a spin pair i, m ($q = 0, \pm 1, \pm 2$).[12]

A first approach to calculate these correlation functions for the case of nuclear-spin relaxation due to the random migration of two types of point defects was recently presented by Cavelius[13] for the case of single and divacancy mechanisms. However, this method starts from the encounter model[7] in its first quantitative formulation,[14] hence neglecting the effect of pair correlations and assuming nondiscrete jump directions of the atoms in a crystal lattice. These simplifications exclude its application to single crystals and make the quantitative comparison of diffusion coefficients determined from NMR experiments with those measured directly, e.g., by means of radioactive tracers questionable.

The difficulties of the encounter model in its first form[14] have been overcome in a more recent article.[8] Therefore, in the present paper, the method developed in Ref. 8 to calculate the correlation functions for a *single* point-defect diffusion mechanism will be extended to account for the effect of *two* diffusion mechanisms relaxing the nuclear-spin system simultaneously.

II. DIPOLAR CORRELATION FUNCTIONS ASSOCIATED WITH TWO POINT-DEFECT DIFFUSION MECHANISMS IN CRYSTALS

Denoting the formation energies of two kinds of point defects (e.g., single and double vacancies) by E_1^F and E_2^F, at a given temperature T their thermal-equilibrium concentrations C_1 and C_2 are given by[1]

$$C_\alpha = C_\alpha^0 e^{-E_\alpha^F/kT} \quad (\alpha = 1, 2) \,. \tag{2.1}$$

Characterized by the migration energies E_1^M and E_2^M, respectively, these defects are assumed to move randomly in the crystal lattice thus causing atomic jumps. Here, C_α^0 represents constants governed by the particular mechanisms.[1]

A. Application of the encounter model

The general procedure of determining dipolar correlation functions starts from the conversion of the time average in Eq. (1.4) into an ensemble average.[15] Hence,

$$G^{(q)}(t) = \sum_{\vec{r}_m^0} F_{im}^{(q)}(\vec{r}_m^0) \sum_{\vec{r}_m^*} P(\vec{r}_m^0, \vec{r}_m^*, t)\, F_{im}^{(q)*}(\vec{r}_m^0 + \vec{r}_m^*) \,, \tag{2.2}$$

where $P(\vec{r}_m^0, \vec{r}_m^*, t)$ denotes the probability that the vector of the relative displacement of an arbitrary spin pair i-m after the time t is equal to $\vec{r}_m^*$, if at $t = 0$ the vector from i (assumed to sit at the origin) to m is $\vec{r}_m^0$.

Once a point defect induces relative jumps of some spin pair i-m, these jumps will occur shortly after the initial jump; they will be bunched into groups.[7] Therefore, if both defect concen-

trations are low enough to avoid interactions between different point defects, the relative motions of the spins "seen" in a relaxation experiment may be broken down into a random sequence of *encounters* with the two types of defects.

Applying this so-called "encounter model" in determining $P(\vec{r}^{\,0}_m, \vec{r}^{\,*}_m, t)$, the time scale may be separated from the geometrical probabilities, by writing

$$P(\vec{r}^{\,0}_m, \vec{r}^{\,*}_m, t) = \sum_{S_1=0}^{\infty} \sum_{S_2=0}^{\infty} q(S_1, S_2, t)\, W_{S_1, S_2}(\vec{r}^{\,0}_m, \vec{r}^{\,*}_m) . \tag{2.3}$$

Here, $q(S_1, S_2, t)$ symbolizes the probability that during the time interval t the spin pair i-m will be rearranged S_1 times by a defect of type 1 *and* S_2 times by a defect of type 2, while $W_{S_1, S_2}(\vec{r}^{\,0}_m, \vec{r}^{\,*}_m)$ accounts for the geometrical probabilities that after an arbitrary sequence of $(S_1 + S_2)$ encounters of the two kinds, the relative displacement vector of the two spins will be $\vec{r}^{\,*}_m$ if the initial vector from i to m is $\vec{r}^{\,0}_m$.

Let us denote the mean time between encounters of i and m with defects of type α by $\tau^{\alpha}_{\mathrm{NMR}}$ $(\alpha = 1, 2)$. Since the two types of rearrangements associated with the two diffusion mechanisms are assumed to be independent of each other, $q(S_1, S_2, t)$ may be decomposed as follows:

$$q(S_1, S_2, t) = w_{S_1}(t, \tau^1_{\mathrm{NMR}})\, w_{S_2}(t, \tau^2_{\mathrm{NMR}}) . \tag{2.4}$$

Here $w_{S_\alpha}(t, \tau^{\alpha}_{\mathrm{NMR}})$ denotes the probability that in time t there are S_α encounters of type α.

At the usually low thermally-created point-defect concentrations, (even at temperatures close to the melting point), the time interval Δt during which the atoms are actually being rearranged during an encounter is much shorter than the mean times $\tau^{\alpha}_{\mathrm{NMR}}$ between encounters. Hence, the Poisson distributions

$$w_{S_\alpha}(t, \tau^{\alpha}_{\mathrm{NMR}}) = \frac{1}{S_\alpha !} \left(\frac{t}{\tau^{\alpha}_{\mathrm{NMR}}} \right)^{S_\alpha} \exp\left(- \frac{t}{\tau^{\alpha}_{\mathrm{NMR}}} \right) \quad (\alpha = 1, 2) \tag{2.5}$$

determine the random sequence of encounters. Inserting Eqs. (2.3)–(2.5) into Eq. (2.2) we obtain

$$G^{(q)}(t) = \sum_{\vec{r}^{\,0}_m} \sum_{S_1=0}^{\infty} \sum_{S_2=0}^{\infty} \frac{R^{(q)}_{S_1, S_2}(\vec{r}^{\,0}_m)}{S_1 ! S_2 !} \frac{t^{S_1+S_2}}{(\tau^1_{\mathrm{NMR}})^{S_1} (\tau^2_{\mathrm{NMR}})^{S_2}} \times \exp\left[- t \left(\frac{1}{\tau^1_{\mathrm{NMR}}} + \frac{1}{\tau^2_{\mathrm{NMR}}} \right) \right] , \tag{2.6}$$

where the lattice terms $R^{(q)}_{S_1, S_2}(\vec{r}^{\,0}_m)$ were defined as follows:

$$R^{(q)}_{S_1, S_2}(\vec{r}^{\,0}_m) = F^{(q)}_{im}(\vec{r}^{\,0}_m) \sum_{\vec{r}^{\,*}_m} W_{S_1, S_2}(\vec{r}^{\,0}_m, \vec{r}^{\,*}_m) \times F^{(q)*}_{im}(\vec{r}^{\,0}_m + \vec{r}^{\,*}_m) . \tag{2.7}$$

Every spin pair in the crystal experiences its individual mixed random sequence of encounters of the two types. Therefore, by defining b_α as the probability that some *encounter* of the spin pair i-m is of type α, the probabilities $W_{S_1, S_2}(\vec{r}^{\,0}_m, \vec{r}^{\,*}_m)$ that a *particular* sequence of S_1 encounters of type 1 *and* S_2 encounters of type 2 leads to a certain geometrical rearrangement may be replaced by the probabilities $W_{S_1+S_2}(\vec{r}^{\,0}_m, \vec{r}^{\,*}_m)$ governed only by the *total* number, $S_1 + S_2$, of encounters experienced by this spin pair. The particular sequence of encounters of the two kinds is thus irrelevant.

Characterizing the geometrical rearrangement resulting from one single encounter of i and m with a defect of type α by the probabilities $P_\alpha(\vec{r}^{\,0}_m, \vec{r}^{\,*}_m)$, for $S_1 + S_2 = 1$ we may write

$$W_1(\vec{r}^{\,0}_m, \vec{r}^{\,*}_m) = b_1 P_1(\vec{r}^{\,0}_m, \vec{r}^{\,*}_m) + b_2 P_2(\vec{r}^{\,0}_m, \vec{r}^{\,*}_m) . \tag{2.8}$$

In complete analogy to the procedure illustrated in Ref. 8, for any value of $S_1 + S_2 > 1$ the probabilities $W_{S_1+S_2}(\vec{r}^{\,0}_m, \vec{r}^{\,*}_m)$ may be calculated successively from the recursion formula

$$W_{S_1+S_2}(\vec{r}^{\,0}_m, \vec{r}^{\,*}_m) = \sum_{\vec{r}^{\,*}} W_{S_1+S_2-1}(\vec{r}^{\,0}_m, \vec{r}^{\,*}) \times W_1(\vec{r}^{\,0}_m + \vec{r}^{\,*}, \vec{r}^{\,*}_m - \vec{r}^{\,*}) , \tag{2.9}$$

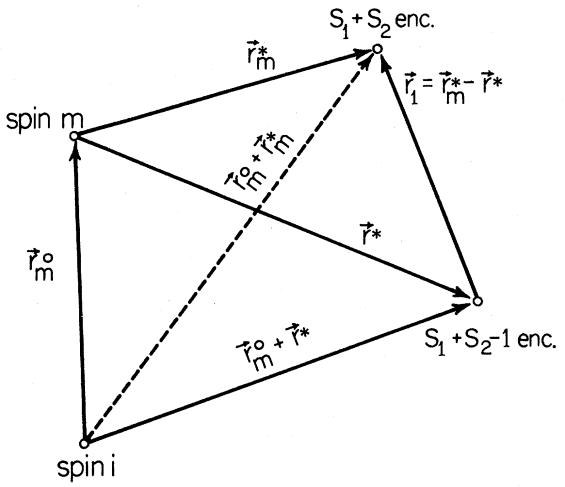

FIG. 1. Initially spin i and spin m are assumed to sit at the origin and at $\vec{r}^{\,0}_m$, respectively. Their "relative displacement vector" due to S_1 encounters of type 1 *and* S_2 encounters of type 2 is denoted by $\vec{r}^{\,*}_m$, and for $S_1 + S_2 - 1$ encounters by $\vec{r}^{\,*}$, respectively. Vector $\vec{r}_1$ characterizes the jump probabilities of the two spins in one encounter averaged over the two types of rearrangements.

taking into account the decrease of pair correlations[8] with increasing number S_1+S_2 of encounters of the two types. The meaning of the vectors involved is illustrated in Fig. 1. Assuming the probabilities b_α and $P_\alpha(\vec{r}^{\,0}_m, \vec{r}^{\,*}_m)$ to be normalized, it is readily seen that the probabilities $W_1(\vec{r}^{\,0}_m, \vec{r}^{\,*}_m)$ and $W_{S_1+S_2}(\vec{r}^{\,0}_m, \vec{r}^{\,*}_m)$ are normalized also, because

$$\sum_{\vec{r}^{\,*}_m} W_1(\vec{r}^{\,0}_m, \vec{r}^{\,*}_m) = \sum_{\alpha=1}^{2} b_\alpha \sum_{\vec{r}^{\,*}_m} P_\alpha(\vec{r}^{\,0}_m, \vec{r}^{\,*}_m) = 1 . \tag{2.10}$$

The total number of *encounters* per second of the spin pair i-m with the two kinds of defects may be written as the sum

$$\frac{1}{\tau_{\mathrm{NMR}}} = \frac{1}{\tau^1_{\mathrm{NMR}}} + \frac{1}{\tau^2_{\mathrm{NMR}}} \tag{2.11}$$

of the encounters of the two individual types. Let us define the probabilities p_α that the *jumps* of some atom are due to a defect of type α, as the average number of atomic jumps per unit time due to *all* defects of type α divided by the total number of atomic jumps per unit time, i.e.,

$$p_\alpha = C_\alpha \nu_\alpha / (C_1\nu_1 + C_2\nu_2) . \tag{2.12}$$

Here ν_α denotes the jump frequencies of defects of type α, while N accounts for the number of atoms in the crystal. Then, the number of *encounters* per second of the spin pair i-m which are of type α may be written as the number of *jumps* per unit time, $2p_\alpha/\tau$, of the two spins induced by type-α defects, divided by the average number of relative jumps of i and m in such an encounter, according to

$$\frac{1}{\tau^\alpha_{\mathrm{NMR}}} = \frac{2p_\alpha}{\tau} \frac{1}{Z_\alpha(0) + Z_\alpha(\vec{r}^{\,0}_m)} = \frac{p_\alpha}{(\tau_{\mathrm{NMR}})_\alpha} . \tag{2.13}$$

Here, $(\tau_{\mathrm{NMR}})_\alpha$ denotes the mean time between two encounters *if* mechanism α is activated alone,[8] while $Z_\alpha(0)$ defines the mean number of jumps of spin i in this type of encounter. $Z_\alpha(\vec{r}^{\,0}_m)$ symbolizes the average number of pair-correlated jumps of spin m in the same encounters. As discussed in Ref. 8, with increasing number of encounters the distance between i and m increases on the average. Therefore $Z_\alpha(\vec{r}^{\,0}_m)$ is a function of the total number of encounters, S_1+S_2, experienced by the spins i and m. Consequently, $\tau^\alpha_{\mathrm{NMR}}$ defined by Eq. (2.13) depends not only on the initial vector $\vec{r}^{\,0}_m$ connecting i and m but also on S_1+S_2.

Similarly as described in Ref. 8, starting from the values of $Z^{(1)}_\alpha(\vec{r}^{\,0}_m)$ determined by a single encounter, the mean number of relative jumps of i and m, $Z_\alpha(0) + Z^{(S_1+S_2)}_\alpha(\vec{r}^{\,0}_m)$ averaged over S_1+S_2 encounters of type α, may be determined from the recursion formula[8]

$$Z_\alpha(0) + Z^{(S_1+S_2)}_\alpha(\vec{r}^{\,0}_m) = \frac{1}{(S_1+S_2)} \left((S_1+S_2-1)[Z_\alpha(0) + Z^{(S_1+S_2-1)}_\alpha(\vec{r}^{\,0}_m)] + Z_\alpha(0) + \sum_{\vec{r}^{\,*}} W_{S_1+S_2}(\vec{r}^{\,0}_m, \vec{r}^{\,*}_m)\, Z_\alpha(\vec{r}^{\,0}_m + \vec{r}^{\,*}_m) \right) , \tag{2.14}$$

with the probabilities $W_{S_1+S_2}(\vec{r}^{\,0}_m, \vec{r}^{\,*}_m)$ given by Eq. (2.9). The vectors used here have been defined in Fig. 1.

According to Eqs. (2.7) and (2.9), the lattice factors $R_{S_1,S_2}(\vec{r}^{\,0}_m)$ depend only on the sum, S_1+S_2, but not on the individual sequence of encounters experienced by a particular spin pair. As illustrated above, the same is true for the parameters $\tau^\alpha_{\mathrm{NMR}}$ in Eq. (2.13); i.e.,

$$\tau^{(\alpha)}_{\mathrm{NMR}}(S_1,S_2) \equiv \tau^{(\alpha)}_{\mathrm{NMR}}(S_1+S_2); \quad R^{(q)}_{S_1,S_2}(\vec{r}^{\,0}_m) = R^{(q)}_{S_1+S_2}(\vec{r}^{\,0}_m) . \tag{2.15}$$

Using these relations and the abbreviation $S = S_1+S_2$, and inserting Eq. (2.11), the correlation functions (2.6) become:

$$G^{(q)}(t) = \sum_{\vec{r}^{\,0}_m} \sum_{S=0}^{\infty} \frac{R^{(q)}_S(\vec{r}^{\,0}_m)}{S!} \exp\left(-\frac{t}{\tau_{\mathrm{NMR}}}\right) \times \sum_{S_1=0}^{\infty} \binom{S}{S_1} [\tau^1_{\mathrm{NMR}}(S)]^{-S_1} [\tau^2_{\mathrm{NMR}}(S)]^{-S+S_1} . \tag{2.16}$$

In writing Eq. (2.16), the binomial coefficients

$$\binom{S_1+S_2}{S_2} = \frac{(S_1+S_2)!}{S_1!\,S_2!}$$

have been introduced.

The case $S=0$ requires some special attention because $\tau^\alpha_{\mathrm{NMR}}$ $(S=0)$ has not been defined so far. If $\tau^\alpha_{\mathrm{NMR}}$ is a function of S, the probabilities $q(0,0,t)$ are not included as the special case for $S_1=S_2=0$ in Eqs. (2.4) and (2.5). Instead, the probability that *no* encounter occurs in time t has to be calculated from the relation[8]

$$q(0,0,t) = 1 - \sum_{S_1=1}^{\infty} \sum_{S_2=1}^{\infty} w_{S_1}(t, \tau^1_{\mathrm{NMR}}(S_1+S_2)) \times w_{S_2}(t, \tau^2_{\mathrm{NMR}}(S_1+S_2)) . \tag{2.17}$$

Inserting the Poisson distributions (2.5) and adopting the procedure illustrated in Ref. 8, it may be shown that in a good approximation

$$q(0,0,t) \approx \exp\{-[\tau^1_{\mathrm{NMR}}(1) + \tau^2_{\mathrm{NMR}}(1)]^{-1}\} . \tag{2.18}$$

Therefore, Eq. (2.16) remains correct if $\tau^{\alpha}_{\mathrm{NMR}}(0)$ is identified with $\tau^{\alpha}_{\mathrm{NMR}}(1)$.

Using Eq. (2.11), the summation over S_1 in Eq. (2.16) is found to be equal to $(\tau_{\mathrm{NMR}})^S$, and the correlation functions $G^{(q)}(t)$ become

$$G^{(q)}(t)=\sum_{\vec{r}^{\,0}_m}\sum_{S=0}^{\infty}\frac{R_S^{(q)}(\vec{r}^{\,0}_m)}{S!}\left(\frac{t}{\tau^{(S)}_{\mathrm{NMR}}}\right)^S\exp\left(-\frac{t}{\tau^{(S)}_{\mathrm{NMR}}}\right), \tag{2.19}$$

where the index S in $\tau^{(S)}_{\mathrm{NMR}}$ indicates the dependence of τ_{NMR} on S (see above), and the lattice terms $R_S^{(q)}(\vec{r}^{\,0}_m)$ were defined by [cf. Eq. (2.7)]:

$$R_S^{(q)}(\vec{r}^{\,0}_m)=F_{im}^{(q)}(\vec{r}^{\,0}_m)\sum_{\vec{r}^{\,*}_m}W_S(\vec{r}^{\,0}_m,\vec{r}^{\,*}_m)\,F_{im}^{(q)*}(\vec{r}^{\,0}_m+\vec{r}^{\,*}_m). \tag{2.20}$$

Via Eqs. (2.8) and (2.9), $R_S^{(q)}(\vec{r}^{\,0}_m)$ is a function of the probabilities b_α. Similarly, via Eqs. (2.11) and (2.13), $\tau^{(S)}_{\mathrm{NMR}}$ in the correlation functions (2.19) depends on the probabilities p_α. As illustrated below, both $G^{(q)}(t)$ and $R_S^{(q)}(\vec{r}^{\,0}_m)$ are therefore *explicitly* temperature dependent.

B. Relation between jumps and encounters

In terms of the probabilities b_α defined above, the total number of encounters per second of the spin pair i-m may be defined in a way slightly different from Eqs. (2.11) and (2.13), by dividing their total number of *jumps* per unit time, $2/\tau$, by their average number of relative jumps in one *encounter* averaged over the two possible types, according to

$$\frac{1}{\tau^{(S)}_{\mathrm{NMR}}}=\frac{2}{\tau}\left(\sum_{\alpha=1}^{2}b_\alpha[Z_\alpha(0)+Z_\alpha^{(S)}(\vec{r}^{\,0}_m)]\right)^{-1}. \tag{2.21}$$

From the first definition of τ_{NMR} [see Eqs. (2.11) and (2.13)] we have

$$\frac{1}{\tau^{(S)}_{\mathrm{NMR}}}=\frac{2}{\tau}\sum_{\alpha=1}^{2}\frac{p_\alpha}{Z_\alpha(0)+Z_\alpha^{(S)}(\vec{r}^{\,0}_m)}=\sum_{\alpha=1}^{2}\frac{p_\alpha}{(\tau^{(S)}_{\mathrm{NMR}})_\alpha}. \tag{2.22}$$

For the two definitions to be completely equivalent b_α and p_α must be related as follows [see Eqs. (2.21) and (2.22)]:

$$b_\alpha=p_\alpha\Big/\frac{Z_\alpha(0)+Z_\alpha^{(S)}(\vec{r}^{\,0}_m)}{Z_1(0)+Z_1^{(S)}(\vec{r}^{\,0}_m)}\left[1+\left(\frac{Z_1(0)+Z_1^{(S)}(\vec{r}^{\,0}_m)}{Z_2(0)+Z_2^{(S)}(\vec{r}^{\,0}_m)}-1\right)p_2\right] \qquad (\alpha=1,2). \tag{2.23}$$

The validity of Eq. (2.23) may be checked by deriving independent expressions for b_α and p_α for a given set of diffusion coefficients D_α ($\alpha=1,2$). For that purpose, the definition (2.12) of p_α may be rewritten, introducing the following general form of the partial diffusion coefficients[1]:

$$D_\alpha=C_\alpha\nu_\alpha g_\alpha d^2. \tag{2.24}$$

Here d denotes the distance between atoms on nearest-neighbor positions in the crystal, while g_α represents geometrical factors to be determined from the explicit evaluation of the Einstein-Smoluchovsky relation (1.3) for mechanism α in a given crystal lattice. Inserting Eq. (2.24) into Eq. (2.12) we obtain

$$p_\alpha=\frac{D_\alpha}{D_\alpha+(g_\alpha/g_\beta)D_\beta}=\frac{D_{0\alpha}e^{-E_\alpha/kT}}{D_{0\alpha}e^{-E_\alpha/kT}+D_{0\beta}(g_\alpha/g_\beta)e^{-E_\beta/kT}} \qquad (\alpha,\beta=1,2;\ \beta\neq\alpha), \tag{2.25}$$

where Eq. (1.1) has been applied. The validity of the normalization condition $p_1+p_2=1$ is readily verified for this form of p_α.

Analogously to Eq. (2.12), the probabilities b_α are defined as the number of encounters per unit time with a defect of type α divided by the total number of encounters of the spin pair i-m during the same time interval; i.e.,

$$b_\alpha=\frac{2C_\alpha\nu_\alpha}{Z_\alpha(0)+Z_\alpha^{(S)}(\vec{r}^{\,0}_m)}\left(\sum_{\beta=1}^{2}\frac{2C_\beta\nu_\beta}{Z_\beta(0)+Z_\beta^{(S)}(\vec{r}^{\,0}_m)}\right)^{-1}. \tag{2.26}$$

Introducing D_α by Eq. (2.24), the probabilities b_α become

$$b_\alpha=D_\alpha\Big/\left(D_\alpha+\frac{g_\alpha}{g_\beta}\,\frac{Z_\alpha(0)+Z_\alpha^{(S)}(\vec{r}^{\,0}_m)}{Z_\beta(0)+Z_\beta^{(S)}(\vec{r}^{\,0}_m)}\,D_\beta\right) \qquad (\alpha,\beta=1,2;\ \beta\neq\alpha), \tag{2.27}$$

from which the validity of the normalization condition $b_1+b_2=1$ is observed. Substituting the form (2.25) of p_α, Eq. (2.23) is readily verified, thus illustrating that Eqs. (2.21) and (2.22) in fact *are* completely identical definitions of $\tau^{(S)}_{\mathrm{NMR}}$.

Noting that the mean number of pair-correlated jumps $Z_\alpha^{(S)}(\vec{r}^{\,0}_m)$ is relatively small compared to the number of jumps $Z_\alpha(0)$, of the "representative" spin i at the origin of our coordinate system, and that the decrease of pair correlations with increasing number of encounters is roughly the same for all diffusion mechanisms,[8,11a] b_α is practically independent of the spin pair i-m considered. Then Eq. (2.27) may be simplified as follows:

$$b_\alpha=D_\alpha\Big/\left(D_\alpha+\frac{g_\alpha}{g_\beta}\,\frac{Z_\alpha(0)}{Z_\beta(0)}\,D_\beta\right)$$

$$=D_{0\alpha}e^{-E_\alpha/kT}\Big/\left(D_{0\alpha}e^{-E_\alpha/kT}+\frac{g_\alpha}{g_\beta}\,\frac{Z_\alpha(0)}{Z_\beta(0)}\,D_{0\beta}e^{-E_\beta/kT}\right) \qquad (\alpha,\beta=1,2;\ \beta\neq\alpha), \tag{2.28}$$

where Eq. (1.1) was used. Similarly, Eq. (2.23) then becomes

$$b_\alpha = p_\alpha \Big/ \left[\frac{Z_\alpha(0)}{Z_\beta(0)} + \left(1 - \frac{Z_\alpha(0)}{Z_\beta(0)}\right) p_\alpha\right] \qquad (\alpha, \beta = 1,2;\ \beta \neq \alpha). \quad (2.29)$$

If all nuclear *jumps* are caused by a defect of type α ($p_\alpha = 1$), all *encounters* must also be of type α ($b_\alpha = 1$). Similarly, for $p_\alpha = 0$ Eq. (2.29) yields $b_\alpha = 0$ as expected. To illustrate the physical meaning of Eq. (2.29), let us consider, e.g., the values of b_α, assuming that equal numbers of nuclear jumps are induced by either type of defects, i.e., that $p_1 = p_2 = 0.5$. Then, if, e.g., $Z_2(0) > Z_1(0)$ there will be *fewer* encounters of the second type ($b_2 < 0.5$) than of the first, since once such an encounter occurs the spins jump more vigorously than in an encounter of the first type. Therefore, Eq. (2.29) predicts $b_1 > 0.5 > b_2$ for $Z_2(0) > Z_1(0)$.

C. Discussion of correlation functions

The correlation functions (2.19) governing the relaxation effects associated with two self-diffusion mechanisms in a single crystal, are characterized by a decaying exponential multiplied by a power series in time. The physical origin of this general mathematical structure was shown to lie in the Poisson distributions [Eq. (2.5)], representing a good approximation as long as the mean time between successive encounters of either type is much longer than the time during which some point defect actually induces the correlated relative jumps of nuclear spins. At the usual thermally created point defect concentrations ($C_\alpha \lesssim 10^{-4}$), this approximation is well justified.

1. Convergence properties

The rapid convergence of the summation over the total number S of encounters in Eq. (2.19) is very closely related to the average increase of the distance between two arbitrary spins and, therefore, the *decrease* of the lattice terms $R_S^{(q)}(\vec{r}_m^{\,0})$ with increasing S. To illustrate this statement, for simplicity let us neglect the relatively small decrease of pair correlations with increasing S, thus assuming $\tau_{\mathrm{NMR}}^{(S)}$ to be effectively independent of S. To obtain an upper limit of the summation over S in Eq. (2.19), all lattice terms $R_S^{(q)}(\vec{r}_m^{\,0})$ may be replaced by their *largest* possible value, namely, the rigid-lattice term $R_{S=0}^{(q)}(\vec{r}_m^{\,0})$. The sum over S then yields an increasing exponential in time, just large enough to compensate the decaying exponential in Eq. (2.19). Obviously, $G^{(q)}(t)$ then no longer decays as a function of time [since $R_S^{(q)}(\vec{r}_m^{\,0})$ no longer decreases with increasing S], but the sum over S still converges. This analysis also illustrates nicely that the origin of the *decay* of $G^{(q)}(t)$ in time originates from the average *decrease* of the dipolar interaction of any pair of spins as a function of time.

2. Special case of only one self-diffusion mechanism activated

The formal identity of the correlation functions (2.19) with those derived earlier[8] for the case where all relative nuclear jumps are due to the random migration of one type of point defects only, is obvious. If only one mechanism, say, number one ($\alpha = 1$) causes diffusion, the temperature-independent values $b_1 = p_1 = 1$ and $b_2 = p_2 = 0$ [see Eq. (2.29)] have to be inserted into Eqs. (2.11) and (2.13) for $\tau_{\mathrm{NMR}}^{(S)}$ and into Eqs. (2.8), (2.9), and (2.20) governing the lattice terms $R_S^{(q)}(\vec{r}_m^{\,0})$. It is readily verified that both $\tau_{\mathrm{NMR}}^{(S)}$ and $R_S^{(q)}(\vec{r}_m^{\,0})$ become completely identical with the expressions derived in Ref. 8; therefore, $G^{(q)}(t)$ given by Eq. (2.19) includes the case of one point-defect mechanism involved as a special case.

Following the discussion in Ref. 8, it is then clear that also the correlation functions associated with a random-walk mechanism of self-diffusion on a crystal lattice[7,15-17] are included in Eq. (2.19) as a special case. Noting that for an uncorrelated mechanism $Z_\alpha(0) = 1$, while pair-correlated jumps do not exist [$Z_\alpha(\vec{r}_m^{\,0}) = 0$], Eq. (2.13) yields $\tau_{\mathrm{NMR}}^{1} = \frac{1}{2}\tau$ independent of S, where S now becomes the number of random relative *jumps* of a pair of spins. Similarly, the probabilities $P_\alpha(\vec{r}_m^{\,0}, \vec{r}_m^{\,*})$ are independent of $\vec{r}_m^{\,0}$ and equal to the inverse of the coordination number G of the crystal, and r_m^* represents one of the G nearest-neighbor lattice vectors $\vec{r}_g$ ($g = 1,2,\ldots,G$). Equation (2.19) then simplifies as follows:

$$G^{(q)}(t) = e^{-2t/\tau} \sum_{S=0}^{\infty} \frac{C^{(q)}(S)}{S!} \left(\frac{2t}{\tau}\right)^S \qquad (2.30)$$

with the lattice sums, e.g., for $S = 1$:

$$C^{(q)}(S=1) = \sum_{\vec{r}_m^{\,0}} F_{im}^{(q)}(\vec{r}_m^{\,0}) \frac{1}{G} \sum_{g=1}^{G} F_{im}^{(q)*}(\vec{r}_m^{\,0} + \vec{r}_g). \qquad (2.31)$$

The random-walk correlation functions (2.30) agree completely with those calculated earlier by Eisenstadt and Redfield,[7] if we limit their results to crystals containing one sort of nuclear spins only. The identity of Eq. (2.30) with Torrey's correlation functions for random-walk diffusion on a space lattice[15] was discussed elsewhere.[16] Performing a powder average of the lattice sums (2.31), Sholl's correlation functions[17] are obtained. As illustrated earlier,[16] this procedure

is not quite legitimate, however, in that it implies that the decay of the sample magnetization of a polycrystalline or powdered sample is simply exponential, as in a single crystal.[16]

III. SPECTRAL DENSITY FUNCTIONS FOR TWO SELF-DIFFUSION MECHANISMS

A. Basic form

The Fourier spectra $J^{(q)}(\omega)$ of the correlation functions (2.19) are readily found to have the following general form (cf. Refs. 8 and 16):

$$J^{(q)}(\omega)=\frac{1}{\omega}\sum_{S=0}^{\infty}\sum_{\vec{r}_m^0}R_S^{(q)}(\vec{r}_m^0)\,j_S(\omega\tau_{\mathrm{NMR}}^{(S)}), \tag{3.1}$$

where the functions $j_S(x)$ were defined in the usual way[8,16] by

$$j_S(x)=\mathrm{Re}[2x/(1-ix)^{S+1}]. \tag{3.2}$$

Re defines the *real* part, and $x=\omega\tau_{\mathrm{NMR}}^{(S)}$ is closely related to Eq. (2.22).

As discussed in Sec. II, a steady increase of the probabilities p_2 and b_2 from zero to one (corresponding to the decrease of b_1 and p_1 from one to zero) is expected to result in a smooth transition of the correlation functions $G^{(q)}(t)$ from their form governed by mechanism 1 to their properties associated with mechanism 2. An analogous transition between their forms $J_1^{(q)}(\omega)$ and $J_2^{(q)}(\omega)$, therefore, also has to occur in the spectral density functions (3.1). This steady transition may be attributed to two effects: (i) the continuous shift of the microscopic time scale, $\tau_{\mathrm{NMR}}^{(S)}$, from $(\tau_{\mathrm{NMR}}^{(S)})_1$ to $(\tau_{\mathrm{NMR}}^{(S)})_2$ [see Eq. (2.22)]. (ii) The steady variation of geometrical probabilities $W_S(\vec{r}_m^0,\vec{r}_m^*)$ due to the variation of $W_1(\vec{r}_m^0,\vec{r}_m^*)$ between $P_1(\vec{r}_m^0,\vec{r}_m^*)$ and $P_2(\vec{r}_m^0,\vec{r}_m^*)$ [see Eqs. (2.8) and (2.9)]; this in turn produces a smooth transition of the lattice factors $R_S^{(q)}(\vec{r}_m^0)$ in Eq. (3.1) from their forms $[R_S^{(q)}(\vec{r}_m^0)]_1$, to $[R_S^{(q)}(\vec{r}_m^0)]_2$ associated with one mechanism acting alone.

Figure 2 represents a doubly logarithmic plot of $J^{(1)}(\omega)$ vs $\omega\tau$ for the mono- and divacancy mechanisms of self-diffusion in a fcc lattice ($p_1=1$ and $p_1=0$, respectively), and for the case in which $p_1=p_2=0.5$ was assumed in the enitre region. (The numerical procedure leading to Fig. 2 is described in Sec. V.) It is obvious from Fig. 2 that the dominant of the two effects mentioned is the first one, producing a shift of the entire curve. Apparently, shape and width of $J^{(q)}(\omega)$ as a function of $\omega\tau$ vary only very little as a function of the parameters b_α and p_α ($\alpha=1,2$). Therefore, the decrease of pair correlations with increasing number S of encounters governed by the probabilities $W_S(\vec{r}_m^0,\vec{r}_m^*)$ [see Eqs. (2.14) and (2.8)] must be approximately equal for both

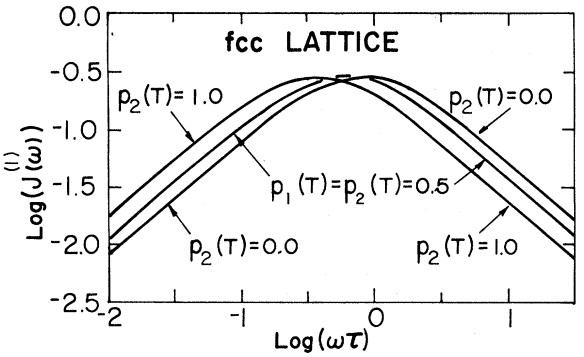

FIG. 2. Doubly logarithmic plot of $J^{(1)}(\omega)$ [given by Eq. (3.1)] vs $\omega\tau$ for a fcc lattice. Shown are the results for monovacancies (Ref. 8) [$p_1(T)=1$], divacancies [$p_2(T)=1$], and for their combined effect for $p_1=p_2=0.5$ independent of temperature. (In units of $\delta\omega^{-1}a_0^{-6}$, where $2a_0$ represents the cube edge of a unit cell.)

mechanisms. This indicates that the second effect outlined above must be very small.

B. Simplifications and approximations

The numerical determination of $J^{(q)}(\omega)$ from Eq. (3.1) for arbitrary values of p_α and b_α is very tedious (see also Sec. V). For practical purposes, it is therefore desirable to simplify Eq. (3.1).

The fact that (i) the shift of the curve for $p_1=p_2=0.5$ in Fig. 2 relative to the plots of $J^{(q)}(\omega)$ for $p_2=0$ and $p_1=0$, respectively, is practically the same on both sides of the maximum of $J^{(q)}(\omega)$, and (ii) shapes and widths of all three curves are about the same, strongly recommends the following decomposition of $J^{(q)}(\omega)$ for *all* values of p_α and b_α:

$$\begin{aligned}J^{(q)}(\omega)&=\sum_{\alpha=1}^{2}p_\alpha J_\alpha^{(q)}(\omega)\\&=\frac{1}{\omega}\sum_{\alpha=1}^{2}p_\alpha\sum_{\vec{r}_m^0}\sum_{S=0}^{\infty}[R_S^{(q)}(\vec{r}_m^0)]_\alpha\,j_S(x_\alpha).\end{aligned} \tag{3.3}$$

Here the lattice terms $[R_S^{(q)}(\vec{r}_m^0)]_\alpha$ and the functions $j_S(x_\alpha)$ associated with the "pure" case of mechanism α acting alone have been introduced, and $x_\alpha=\omega(\tau_{\mathrm{NMR}}^{(S)})_\alpha$.

For $p_1=b_1=0$ and $p_1=b_1=1$, respectively, the unrestricted validity of Eq. (3.3) is readily verified using the general forms (2.19) and (3.1) of $G^{(q)}(t)$ and $J^{(q)}(\omega)$, respectively, together with the general relations (2.20) and (2.22) for the lattice terms and the mean numbers of encounters per unit time. On the low-temperature side of the maximum of $J^{(q)}(\omega)$ ($x\gg1$), Eq. (3.1) yields:

$$J^{(q)}(\omega)=\frac{4}{\omega}\sum_{\vec{r}_m^0}\frac{R_0^{(q)}(\vec{r}_m^0)-R_1^{(q)}(\vec{r}_m^0)}{x}$$
$$=\frac{4}{\omega}\sum_{\alpha=1}^{2}p_\alpha\sum_{\vec{r}_m^0}\frac{[R_0^{(q)}(\vec{r}_m^0)]_\alpha-[R_1^{(q)}(\vec{r}_m^0)]_\alpha}{x_\alpha}\ , \tag{3.4}$$

where $x=\omega\tau_{\mathrm{NMR}}^{(S)}$, and the asymptotic forms of $j_S(x)$ discussed elsewhere[8,16] have been used. Also, according to Eq. (2.22),

$$1/x=p_1/x_1+p_2/x_2\ . \tag{3.5}$$

In writing Eq. (3.4), the following form of $R_S^{(q)}(\vec{r}_m^0)$ for $S=0$ and $S=1$ was used [see Eqs. (2.20) and (2.8)]:

$$R_S^{(q)}(\vec{r}_m^0)=b_1[R_S^{(q)}(\vec{r}_m^0)]_1+b_2[R_S^{(q)}(\vec{r}_m^0)]_2\quad(S=0,1)\ . \tag{3.6}$$

As discussed above, $R_S^{(q)}(\vec{r}_m^0)$ varies only very little as a function of the probabilities b_α. Therefore, the asymptotic form (3.4) of $J^{(q)}(\omega)$ represents a very good approximation. Comparing Eqs. (3.4) and (3.3), it is seen that on the low-temperature side of the $J^{(q)}(\omega)$ maximum, the approximation (3.3) introduced on phenomenological grounds is practically identical with the exact form (3.1) for all values of p_1 and p_2.

On the high-temperature side of the maximum of $J^{(q)}\omega$ ($x\ll 1$), the general validity of the approximation (3.3) cannot be derived from Eq. (3.1) for all values of p_1 and p_2. Only for $p_1\lesssim 1$ and $p_2\lesssim 1$, respectively, Eq. (3.3) is found to be a very good approximation to the exact form (3.1). Nevertheless, as we shall show in Sec. V, even for intermediate values of p_1 and p_2, Eq. (3.3) represents a fairly good approximation, certainly good enough for all practical purposes.

IV. TEMPERATURE DEPENDENCE AND ANISOTROPY OF RELAXATION RATES

Using the spectral density functions (3.1) or their simplified version (3.3), respectively, all relaxation properties (anisotropy, temperature, and field dependence of relaxation rates) associated with two self-diffusion mechanisms may be predicted. Inserting Eq. (3.1) into the usual expressions for T_1 and T_2 (see, e.g., Abragam[12]), we obtain

$$\frac{1}{T_1}=\frac{3\delta}{2}\sum_{q=1}^{2}\frac{1}{q\omega_0}\sum_{S=0}^{\infty}\sum_{\vec{r}_m^0}R_S^{(q)}(\vec{r}_m^0)\,j_S(q\omega_0\tau_{\mathrm{NMR}}^{(S)})\ , \tag{4.1}$$

$$\frac{1}{T_2}=\frac{3\delta}{8}\sum_{S=0}^{\infty}\sum_{\vec{r}_m^0}\left(2R_S^{(0)}(\vec{r}_m^0)\,\tau_{\mathrm{NMR}}^{(S)}+\sum_{q=1}^{2}\frac{h^{(q)}}{q\omega_0}R_S^{(q)}(\vec{r}_m^0)\,j_S(q\omega_0\tau_{\mathrm{NMR}}^{(S)})\right). \tag{4.2}$$

Similarly, using Look and Lowe's relation,[18,19] in the high-field limit the corresponding expression for $T_{1\rho}$ becomes

$$\frac{1}{T_{1\rho}}=\frac{3\delta}{8}\sum_{q=0}^{2}\sum_{S=0}^{\infty}\sum_{\vec{r}_m^0}\frac{h^{(q)}}{\omega^{(q)}}R_S^{(q)}(\vec{r}_m^0)\,j_S(\omega^{(q)}\tau_{\mathrm{NMR}}^{(S)})\ , \tag{4.3}$$

with $\delta=\gamma^4\hbar^2I(I+1)$ and the following abbreviations:

$$h^{(0)}=h^{(2)}=1;\quad h^{(1)}=10;\quad \omega^{(0)}=2\omega_1;\ \omega^{(q)}=q\omega_0\quad(q=1,2)\ . \tag{4.4}$$

Owing to the linearity of the relation between the relaxation rates T_r^{-1} and the spectral density functions $J^{(q)}(\omega)$, it is obvious that their simplified form (3.3) leads to the following linear decomposition:

$$1/T_{\mathrm{rel}}=p_1(1/T_{\mathrm{rel}})_1+p_2(1/T_{\mathrm{rel}})_2\ , \tag{4.5}$$

where $(T_{\mathrm{rel}}^{-1})_\alpha$ symbolizes the relaxation rates associated with the "pure" case of mechanism α ($\alpha=1,2$) alone causing self-diffusion (see, e.g., Ref. 8).

In what follows, temperature dependence and anisotropy of the relaxation times T_1, T_2, and $T_{1\rho}$ will be analyzed for both the exact relations [Eqs. (4.1)–(4.3)] and their simplified versions (4.5).

A. Temperature dependence

Through the mean jump time τ and the probabilities p_α and b_α, the relaxation times T_1, T_2, and $T_{1\rho}$ vary with temperature. Applying the Einstein-Smoluchovsky relation (1.3) to Eq. (1.1) and introducing the parameters

$$D_{\alpha\beta}=\frac{D_{0\alpha}}{D_{0\beta}},\quad \epsilon=\frac{E_2-E_1}{E_1},\quad g_{\alpha\beta}=\frac{g_\alpha}{g_\beta}\quad(\alpha,\beta=1,2;\ \beta\neq\alpha)\ , \tag{4.6}$$

the mean jump time τ varies with temperature according to

$$\frac{1}{\tau}=\frac{6D_{01}}{d^2}e^{-E_1/kT}(1+D_{21}e^{-\epsilon E_1/kT})\ . \tag{4.7}$$

Similarly, in terms of the parameters (4.6), the probability p_2, e.g., depends on temperature in the following fashion [see Eq. (2.25)]:

$$p_2(T)=\frac{g_{12}D_{21}e^{-\epsilon E_1/kT}}{1+g_{12}D_{21}e^{-\epsilon E_1/kT}}\,, \tag{4.8}$$

while $p_1(T)$ may be determined from the normalization condition: $p_1=1-p_2$. Finally, the temperature variation of the probabilities b_α is governed by Eqs. (2.29) or (2.28), respectively.

Inserting Eqs. (4.7), (4.8), and (2.29) into Eqs. (4.1)–(4.3) and (4.5), respectively, the temperature dependence of T_1, T_2, and $T_{1\rho}$ may be determined in the exact limit and under the assumptions underlying the approximate form (3.3) of the spectral densities. As illustrated in Sec. V, this requires the evaluation of the lattice sums involved for each particular combination of diffusion mechanisms.

B. Orientation dependence of relaxation rates in cubic single crystals

As a function of the orientation of the strong constant magnetic field $\vec{H}_0$ with respect to the main cubic crystal axes (characterized by two angles, θ and ϕ)[16], the lattice terms $R_S^{(q)}(\vec{r}_m^{\,0})$ in Eqs. (3.1) and (4.1)–(4.3) vary according to[8,16]

$$R_S^{(q)}(\vec{r}_m^{\,0})=A_S^{(q)}(\vec{r}_m^{\,0})+f(\theta,\phi)\,B_S^{(q)}(\vec{r}_m^{\,0})\,, \tag{4.9}$$

where the "anisotropy function" $f(\theta,\phi)$ is given by[8,16]

$$f(\theta,\phi)=\sin^2 2\theta+\sin^4\theta\sin^2 2\phi\,. \tag{4.10}$$

Via the probabilities $b_\alpha(T)$, the orientation independent new lattice terms $A_S^{(q)}(\vec{r}_m^{\,0})$ and $B_S^{(q)}(\vec{r}_m^{\,0})$ originally defined in Ref. 16 depend on temperature. Only in the limiting case of one diffusion mechanism acting alone, the lattice terms $[A_S^{(q)}(\vec{r}_m^{\,0})]_\alpha$ and $[B_S^{(q)}(\vec{r}_m^{\,0})]_\alpha$ in the expression

$$[R_S^{(q)}(\vec{r}_m^{\,0})]_\alpha=[A_S^{(q)}(\vec{r}_m^{\,0})]_\alpha+f(\theta,\phi)\,[B_S^{(q)}(\vec{r}_m^{\,0})]_\alpha \tag{4.11}$$

governing the simplified relations (3.3) and (4.5), are independent of temperature.

It is well known that the anisotropies of the relaxation rates depend on temperature.[8,11,16] This is illustrated, e.g., in Fig. 3, where T_1^{-1}, T_2^{-1}, and $T_{1\rho}^{-1}$ (for $H_1 \gg H_{1\rho}$) have been plotted versus $\omega_0\tau$ for two different orientations of the field $\vec{H}_0$ with respect to the main crystal axes and for polycrystalline samples. The mechanisms chosen in Fig. 3 are the so-called 1N-2N-4N mechanism of divacancy migration in a bcc lattice and the monovacancy mechanism. (For details, see Sec. V.)

As discussed earlier[8,16] and as also suggested by Fig. 3, for temperatures far below and far above the T_1 and $T_{1\rho}$ minimum, respectively, explicit expressions for the orientation dependences of T_1, T_2, and $T_{1\rho}$ may be derived, starting from Eqs. (4.1)–(4.3) and (4.5), respectively, the form (3.2) of the functions $j_S(x)$, and Eqs. (4.9)–(4.11). This procedure is completely analogous to earlier work,[8,16] and will therefore not be illustrated here in detail. In Sec. V, however, numerical values of these anisotropies in the different temperature regions will be presented. Noting that[8,16]

$$\sum_{\vec{r}_m^{\,0}} B_S^{(2)}(\vec{r}_m^{\,0})=-\sum_{\vec{r}_m^{\,0}} B_S^{(1)}(\vec{r}_m^{\,0})=\frac{1}{9}\sum_{\vec{r}_m^{\,0}} B_S^{(0)}(\vec{r}_m^{\,0}) \tag{4.12}$$

for any self-diffusion mechanism, it may readily be shown, e.g., that on the high-temperature side of the T_1 minimum (i.e., for $\omega_0\tau \ll 1$) Eqs. (4.1)–(4.3) predict T_1, T_2, and $T_{1\rho}$ to be equal and isotropic (see also Refs. 7 and 11b).

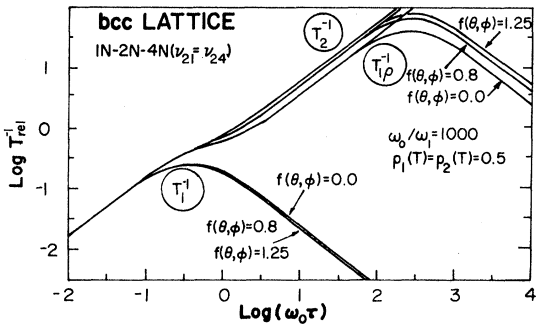

FIG. 3. Relaxation rates for the simultaneous migration of mono- and divacancies (1N-2N-4N, $\nu_{21}=\nu_{24}$, see Sec. V A) in a bcc lattice for $p_1(T)=p_2(T)=0.5$ (independent of temperature) and two different crystallographic orientations of the field $\vec{H}_0$, namely $f(\theta,\phi)=0$ ($\theta=0$, $\phi=0$), $f(\theta,\phi)=1.25$ ($\theta=45°$, $\phi=45°$), and for polycrystalline samples for which $f(\theta,\phi)=0.8$ (Ref. 16). [$\omega_0/\omega_1=1000$, T_1^{-1} and T_2^{-1} in units of $\delta\omega_0^{-1}a_0^{-6}$, $T_{1\rho}^{-1}$ in units of $\delta\omega_1^{-1}a_0^{-6}$; see Eqs. (4.1)–(4.3) with Eqs. (4.9) and (4.10).]

V. NUMERICAL RESULTS FOR VACANCY-INDUCED SELF-DIFFUSION IN fcc AND bcc CRYSTALS

To investigate the relaxation effects of a temperature-dependent admixture of divacancies to the dominant monovacancy mechanisms in fcc and bcc crystals (see Sec. I), in the rest of this article the two relaxation mechanisms will be identified with a mono- and a divacancy mechanism of self-diffusion.

As illustrated above, the numerical determination of the temperature dependence of T_1, T_2, and $T_{1\rho}$ and their anisotropies necessitates the evaluation of the lattice sums $R_S^{(q)}(\vec{r}_m^{\,0})$ and the mean time $\tau_{\rm NMR}^{(S)}$ between encounters. These quantities, in turn, are governed by the geometrical probabilities $P_\alpha(\vec{r}_m^{\,0},\vec{r}_m^{\,*})$ [see Eqs. (2.8), (2.9), and (2.20)]

TABLE I. Comparison of two modes of migration of divacancies in a bcc crystal. Listed is the number of jumps of spin i, $Z_\alpha(0)$ (column 1), and the number of pair-correlated jumps, $Z_\alpha(\vec{r}_m^{\,0})$ of a spin m sitting on a nearest- to third-nearest-neighboring position $\vec{r}_m^{\,0}$ (columns 2 to 4) relative to spin i located at the origin $[\vec{r}_m^{\,0}=(0,0,0)]$. For comparison, results for single vacancies have been included (Ref. 8). The values of $Z_\alpha(0)$ are in agreement with those presented by Cavelius (Ref. 13).

$Z_\alpha(\vec{r}_m^{\,0})$	$\vec{r}_m^{\,0}=(0,0,0)$	$(\pm1,\pm1,\pm1)$	$(0,0,\pm2)$	$(0,\pm2,\pm2)$
Single vacancies (Ref. 8) ($\alpha=1$)	1.36	0.65	0.53	0.41
Divacancies ($\alpha=2$) (1N-2N-1N, i.e., $\nu_{24}=0$)	2.47	1.94	1.78	1.41
Divacancies ($\alpha=2$) (1N-2N-4N for $\nu_{21}=\nu_{24}$)	2.19	1.84	1.69	1.34

and the average number of relative jumps, $Z_\alpha(0)+Z_\alpha(\vec{r}_m^{\,0})$, in an encounter of an arbitrary spin pair with a single or double vacancy. As illustrated earlier,[8,11] numerical values of these parameters may be determined from the computer simulation of the random migration of these defects.

A. Computer simulation of the random migration of mono- and divacancies in fcc and bcc lattices

Numerical values of $P_1(\vec{r}_m^{\,0},\vec{r}_m^{\,*})$ and $Z_1(0)+Z_1(\vec{r}_m^{\,0})$ for self-diffusion via single vacancies by random vacancy jumps to nearest-neighboring positions in fcc and bcc crystals are found in Ref. 8, while results for random nearest-neighbor jumps of divacancies in a *fcc* lattice have been presented in Ref. 11a.

In a *bcc* lattice, the modes of divacancy migration are more complicated. Thus, e.g., a divacancy originally, say, in a nearest-neighbor (1N) configuration (i.e., the two vacancies are sitting at nearest-neighboring positions in the crystal) cannot jump into another 1N configuration without partially dissociating, even though the individual vacancies of the pair are assumed to jump to nearest-neighboring sites only. Therefore, after the jump of one of the two vacancies, the divacancy forms a second-nearest-neighbor (2N) configuration. As pointed out, e.g., by Mehrer,[20] from this 2N configuration the vacancies may either jump back into a 1N configuration (i.e., associate again with a probability ν_{21}) or they may dissociate even further by jumping into a 4N configuration (with probability ν_{24}).

Some typical results for the two divacancy mechanisms in a bcc lattice (so-called 1N-2N-1N and 1N-2N-4N mechanisms) are listed in Tables I–III. They were obtained from the simulation of 1500 encounters in each case, every encounter consisting of 1300 random jumps of a divacancy. All calculations were performed in the CDC 6600 computer of the University of Stuttgart. The computer time required for the simulation of one mechanism amounts to about 8 min. (For details on the computer simulation of the random migration of single and double vacancies in cubic crystals, see Ref. 21.)

The motivation for simulating both the 1N-2N-1N and the 1N-2N-4N mechanism was to find out whether they are distinguishable by NMR studies. To get an idea of the differences expected we have chosen the simple case $\nu_{21}=\nu_{24}$ for the simulation of the 1N-2N-4N mechanism. As seen from Table I, the average numbers of relative jumps are rather different for the two mechanisms; but the decrease of pair correlations with increasing number of encounters is about the same (see Table II).

Although there are fewer correlated jumps of

TABLE II. Decrease of pair correlations with increasing number S of encounters for the monovacancy (Ref. 8) and for two divacancy mechanisms in a bcc lattice. Listed is the total number of relative jumps, $Z_\alpha(0)+Z_\alpha^{(S)}(\vec{r}_m^{\,0})$ of spin i and spin m after S encounters of type α.

$Z_\alpha(0)+Z_\alpha^{(S)}(\vec{r}_m^{\,0})$	$S=1$	$S=2$	$S=3$	$S=4$
Single vacancies (Ref. 8) ($\alpha=1$)	2.02	1.93	1.88	1.84
Divacancies ($\alpha=2$) (1N-2N-1N, i.e., $\nu_{24}=0$)	4.41	4.19	4.02	3.88
Divacancies ($\alpha=2$) (1N-2N-4N for $\nu_{21}=\nu_{24}$)	4.03	3.84	3.69	3.55

TABLE III. Probabilities $P_\alpha(\vec{r}_m^{\,0}, \vec{r}_m^{\,*})$ for mono- and divacancies in a bcc lattice. $\vec{r}_m^{\,0} = (0,0,0)$ represents the position of spin i located at the origin, while $\vec{r}_m^{\,0} = (1,1,1)$ denotes the position of a nearest-neighboring spin of i. (For further details, see Secs. II A and V A.)

$P_\alpha(\vec{r}_m^{\,0}, \vec{r}_m^{\,*})$	$\vec{r}_m^{\,0}$	$\vec{r}_m^{\,*}=(0,0,0)$	$\vec{r}_m^{\,*}=(1,1,1)$	$\vec{r}_m^{\,*}=(0,0,2)$	$\vec{r}_m^{\,*}=(0,2,2)$
Single vacancies	(0,0,0)	12.9	9.6	1.0	0.2
(Ref. 8) ($\alpha=1$)	(1,1,1)	11.8	7.6	1.8	0.6
Divacancies ($\alpha=2$)	(0,0,0)	13.3	7.7	2.7	0.4
(1N-2N-1N, i.e.,	(1,1,1)	9.5	5.9	3.3	0.8
$\nu_{21}=0$)					
Divacancies ($\alpha=2$)	(0,0,0)	11.1	8.5	2.2	0.4
(1N-2N-4N for	(1,1,1)	9.3	6.1	3.2	1.0
$\nu_{21}=\nu_{24}$)					

the spins i and m in an encounter of the 1N-2N-4N type (see Table I), Table III indicates that the spins move apart further than in an encounter of the 1N-2N-1N type. Thus, e.g., the probability $W_1(0,0)$ of spin i remaining at its lattice site is 13.3% for the 1N-2N-1N mechanism versus 11.1% for the 1N-2N-4N mechanism. Similarly, the probabilities of greater relative displacements of two nearest-neighboring spins are higher for the second mechanism.

Unfortunately, see Sec. V B, in their effect on the relaxation rates the differences between the two divacancy mechanisms exhibited by Tables I–III tend to compensate each other.

B. Anisotropies of relaxation rates for single- and double-vacancy migration in fcc and bcc crystals

Starting from the explicit expressions of the orientation-independent lattice terms $A_S^{(q)}(\vec{r}_m^{\,0})$ and $B_S^{(q)}(\vec{r}_m^{\,0})$ in terms of the crystallographic coordinates (x_m^0, y_m^0, z_m^0) of $\vec{r}_m^{\,0}$ (see Ref. 16), the anisotropies of T_1, T_2, and $T_{1\rho}$ in the different temperature regimes may be calculated, making use of the recursive procedure for the evaluation of the average number of relative jumps, $Z(0) + Z^{(S)}(\vec{r}_m^{\,0})$ of the spin-pair i-m and the geometrical probabilities $W_S(\vec{r}_m^{\,0}, \vec{r}_m^{\,*})$ associated with S encounters [see Eqs. (2.9) and (2.14)]. Results of these rather lengthy computer calculations are listed in Table IV.

As discussed elsewhere,[8,16,11b] T_1 and $T_{1\rho}$ for $\omega_0\tau \gg 1$ and $\omega_1\tau \gg 1$, respectively, are fully determined by the terms for $S=0$ and $S=1$ in Eqs. (4.1)–(4.3) alone. In contrast, the values of $T_{1\rho}$ for $\omega_1\tau \ll 1$, of T_1 for $\omega_0\tau \ll 1$, and of T_2 in the entire (motionally narrowed) temperature region are governed by *many* encounters. The required computer time in these regions is, therefore, determined by the convergence of the summations over S in Eqs. (4.1)–(4.3), which included as many as $S_{\max}=10$ encounters for the results listed in lines 3 and 4 of Table IV. Typical computer times were about 50 to 60 min on a CDC 6600 computer, compared to only about 6 min for the results in lines 1 and 2 involving terms for $S=0$ and $S=1$ only. A further increase of $S_{\max}$ left these results practically unchanged. All lattice sums were extended over the first 1350 spins closest to the "representative" spin i at the origin.

The function $f(\theta,\phi)$ may vary between 0 and $\frac{4}{3}$ [see Eq. (4.10)], its smallest value corresponding to the orientation of $\vec{H}_0$ parallel to a $\langle 100\rangle$ direction of the cubic crystal, and its largest value defining a $\langle 111\rangle$ orientation of $\vec{H}_0$. The *"anisotropy factor"* Δ, defined by

$$\Delta = \frac{T_{\rm rel}[f(\theta,\phi)=\frac{4}{3}] - T_{\rm rel}[f(\theta,\phi)=0]}{T_{\rm rel}[f(\theta,\phi)=0]} = \frac{T_{\rm rel}(\langle 111\rangle) - T_{\rm rel}(\langle 100\rangle)}{T_{\rm rel}(\langle 100\rangle)}, \tag{5.1}$$

therefore represents a convenient measure for the orientation dependence of the relaxation times T_1, T_2, and $T_{1\rho}$. Values of Δ for the different vacancy mechanisms have been included in Table IV.

The relatively small differences of the anisotropies of T_1 and T_2 for $\omega_0\tau \gg 1$ associated with the two modes of divacancy migration in a bcc lattice are illustrated in Fig. 4.

C. Discussion of anisotropies

From Table IV and Fig. 4, it is apparent that the orientation dependences of T_1, T_2, and $T_{1\rho}$ for the vacancy mechanisms considered are too similar to be experimentally distinguishable. Reasons therefore lie in the fact that (i) the geometrical rearrangements of two spins due to the random jumps of different kinds of vacancies are very

TABLE IV. Anisotropies of the relaxation rates T_1^{-1}, T_2^{-1}, and $T_{1\rho}^{-1}$ for the change of the dominant diffusion mechanism from single vacancies (column 1) to double vacancies (column 4) in fcc and bcc lattices. Column 2 shows the results of the exact evaluation of Eqs. (4.1)–(4.3) for $p_1(T)=p_2(T)=0.5$ (independent of temperature), while the values in column 3 were obtained from the approximation (4.5) and the values in columns 1 and 4. [$2a_0$ is the cube edge of a unit cell, $\delta=\gamma^4\hbar^2 I(I+1)$.] The anisotropy factor Δ was defined in Sec. V B.

	Lattice type	Single vacancies [$p_1=1$, $p_2=0$; see Eqs. (4.1)–(4.3) and (4.5) and Ref. 8]	Δ(%)	$p_1=p_2=0.5$ Exact results: evaluation of Eqs. (4.1)–(4.2)	Δ (%)	Approximate results: derived from Eq. (4.5) and columns 1 and 4	Δ (%)	Divacancies [$p_1=0$, $p_2=1$; see Eqs. (4.1)–(4.3) and (4.5)]	Δ(%)
$T_{1\rho}^{-1}$ for $H_1 \gg H_{L\rho}$ for $\omega_1\tau \gg 1$ in units of $\delta\omega_1^{-2}\tau^{-1}a_0^{-6}$	fcc	$[0.1737+0.0755f(\theta,\phi)]$	−36.7	$[0.1253+0.0557f(\theta,\phi)]$	−37.2	$[0.1256+0.0553f(\theta,\phi)]$	−37.0	$[0.0775+0.0351f(\theta,\phi)]$	−37.7
	bcc 1N-2N-1N	$[0.0342+0.0266f(\theta,\phi)]$	−50.9	$[0.0253+0.0196f(\theta,\phi)]$	−50.8	$[0.0251+0.0196f(\theta,\phi)]$	−51.0	$[0.0159+0.0125f(\theta,\phi)]$	−51.1
	bcc 1N-2N-4N			$[0.0257+0.0206f(\theta,\phi)]$	−51.7	$[0.0255+0.0205f(\theta,\phi)]$	−51.7	$[0.0168+0.0143f(\theta,\phi)]$	−53.2
T_1^{-1} for $\omega_0\tau \gg 1$ in units of $\delta\omega_0^{-2}\tau^{-1}a_0^{-6}$	fcc	$[1.3287-0.1007f(\theta,\phi)]$	+11.2	$[0.9659-0.0743f(\theta,\phi)]$	+11.4	$[0.9655-0.0737f(\theta,\phi)]$	+11.3	$[0.6024-0.0467f(\theta,\phi)]$	+11.5
	bcc 1N-2N-1N	$[0.3246-0.0355f(\theta,\phi)]$	+17.2	$[0.2392-0.0262f(\theta,\phi)]$	+17.1	$[0.2380-0.0267f(\theta,\phi)]$	+17.1	$[0.1515-0.0167f(\theta,\phi)]$	+17.2
	bcc 1N-2N-4N			$[0.2464-0.0274f(\theta,\phi)]$	+17.4	$[0.2452-0.0273f(\theta,\phi)]$	+17.4	$[0.1658-0.0191f(\theta,\phi)]$	+18.1
$T_{1\rho}^{-1}\equiv T_2^{-1}$ for $H_1 \gg H_{L\rho}$ and $\omega_0\tau \gg 1$, $\omega_1\tau \ll 1$ in units of $\delta\tau a_0^{-6}$	fcc	$[1.1038+0.4057f(\theta,\phi)]$	−32.9	$[1.4875+0.5492f(\theta,\phi)]$	−33.0	$[1.7833+0.6381f(\theta,\phi)]$	−32.3	$[2.3253+0.8704f(\theta,\phi)]$	−33.3
	bcc 1N-2N-1N	$[0.2672+0.1432f(\theta,\phi)]$	−41.7	$[0.3510+0.1933f(\theta,\phi)]$	−42.3	$[0.4018+0.2225f(\theta,\phi)]$	−42.5	$[0.5364+0.3018f(\theta,\phi)]$	−42.9
	bcc 1N-2N-4N			$[0.3442+0.1846f(\theta,\phi)]$	−41.7	$[0.3849+0.2036f(\theta,\phi)]$	−40.9	$[0.5026+0.2639f(\theta,\phi)]$	−41.2
$T_1^{-1}\equiv T_2^{-1}\equiv T_{1\rho}^{-1}$ for $H_0 \gg H_1 \gg H_{L\rho}$ and $\omega_0\tau \ll 1$ in units of $\delta\tau a_0^{-6}$	fcc	4.7630	0.0	6.4240	0.0	7.4039	0.0	10.0448	0.0
	bcc 1N-2N-1N	1.2744	0.0	1.6905	0.0	1.9389	0.0	2.6033	0.0
	bcc 1N-2N-4N			1.6433	0.0	1.8301	0.0	2.3852	0.0

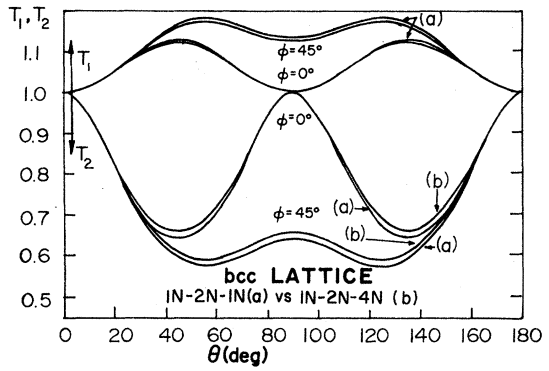

FIG. 4. Anisotropies of T_1 and T_2 for $\omega_0\tau \gg 1$ for the 1N-2N-1N and the 1N-2N-4N ($\nu_{21}=\nu_{24}$) mechanism of divacancy migration in a bcc lattice (in arbitrary units; see lines 2 and 3 of Table IV).

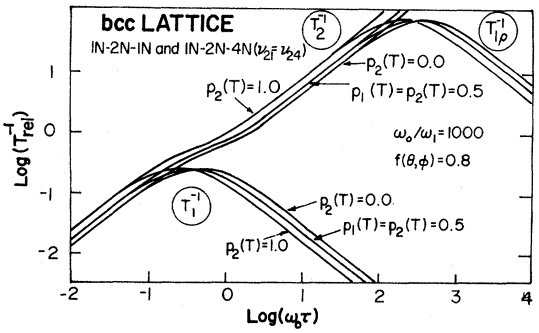

FIG. 5. Doubly-logarithmic plot of T_1^{-1}, T_2^{-1}, and $T_{1\rho}^{-1}$ (for $H_1 \gg H_{L\rho}$) vs $\omega_0\tau$ for powdered bcc samples [$f(\theta,\phi)=0.8$]. The dominant diffusion mechanism was assumed to change from single vacancies ($p_2=0$) through $p_1=p_2=0.5$ to divacancies ($p_2=1$). The plots obtained from the evaluation of Eqs. (4.1)–(4.3) are practically the same for both the 1N-2N-1N and the 1N-2N-4N mechanisms. Units are the same as in Fig. 3. Corresponding numerical values are listed in Table V.

similar, and (ii) the anisotropies of high-field relaxation rates are mainly due to the orientation dependence of the dipolar local field,[11b] incorporated in the rigid-lattice contributions (terms for $S=0$) to the relaxation rates (4.1)–(4.3) and (4.5). The anisotropies of $T_{1\rho}$ in a *low* rotating field in the so-called Slichter-Ailion region are known to be mainly due to the *motions* of spins and not due to the local field. These effects will be the subject of a forthcoming article.

As outlined above, all values listed in columns 1 and 4 of Table IV are independent of whether they were obtained from Eqs. (4.1)–(4.3) or from the approximation (4.5). For $p_1=p_2=0.5$, columns 2 and 3 show the predictions obtained from Eqs. (4.1)–(4.3) and from the simplified relations (4.5), respectively, by superposition of the values in columns 1 and 4. In the temperature regions where only the terms for $S=0$ and $S=1$ contribute to the relaxation process (see lines 1 and 2 of Table IV), the agreement between exact and approximately valid results is excellent. Following the discussion in Sec. III B, this is not surprising. As expected, in the regimes where *many* encounters contribute to relaxation (see lines 3 and 4 of Table IV), the differences between exact and approximate results are greater (typically about 10 to 15%). However, noting that the probabilities p_α and b_α are not known too accurately either (owing to uncertainties in our knowledge of the parameters D_{01}, D_{02}, E_1, E_2), for all practical purposes at all temperatures the simplified relations (4.5) certainly represent good approximations to the more accurate expressions (4.1)–(4.3).

D. Temperature dependence of T_1 and $T_{1\rho}$

Although the anisotropies of the high-field relaxation times are rather insensitive functions of the types of vacancies inducing atomic jumps, their *magnitudes* for a given value of the mean atomic jump time τ may differ considerably. In a more complete way than in Table IV, this effect is illustrated in Fig. 5, showing the relaxation rates in a polycrystalline sample [$f(\theta,\phi)=0.8$] as functions of $\omega_0\tau$ for three temperature-independent values of the parameters p_α and b_α.

In reality, p_α and b_α are functions of temperature [see, e.g., Eqs. (4.8) and (2.28)], an effect not exhibited by plots of the type of Fig. 5.

The transformation of the $\log_{10}(\omega_0\tau)$ scale in Fig. 5 into an inverse-temperature scale is readily accomplished. Following Eq. (4.7), any value of $\log_{10}(\omega_0\tau)$ may be converted, e.g., into a corresponding value of the parameter E_1/kT, according to

$$\log_{10}(\omega\tau) = \log_{10}\left(\frac{\omega d^2}{6D_{01}}\right) + \frac{E_1}{kT}\frac{1}{\ln 10} - \log_{10}(1+D_{21}e^{-\epsilon E_1/kT}) . \tag{5.2}$$

Using the relaxation rates $(T_{\rm rel}^{-1})_\alpha$ ($\alpha=1,2$) shown in Fig. 5 (plots for $p_2=0$ and $p_2=1$, respectively) and listed point by point in Table V and VI for the bcc and the fcc lattice, respectively, as functions of $\log_{10}(\omega\tau)$, and applying the relation [see Eq. (4.5)]

$$1/T_{\rm rel} = p_1(T)\,(1/T_{\rm rel})_1 + p_2(T)\,(1/T_{\rm rel})_2 \tag{5.3}$$

found to be sufficiently accurate in the *entire* temperature range (see above), for any given set of values for ω_0, E_1, D_{01}, ϵ, and D_{21} the temperature dependence of the relaxation rates may be determined from the following procedure:

(i) For any value of E_1/kT, Eq. (5.2) allows

TABLE V. Numerical values of T_1^{-1}, T_2^{-1}, and $T_{1\rho}^{-1}$ as functions of $\log_{10}(\omega_0\tau)$ and $\log_{10}(\omega_1\tau)$, respectively, in the region where the T_1 and $T_{1\rho}$ minima occur, respectively, for the diffusion via single and double vacancies (1N-2N-1N) in a *bcc* lattice. The results for the 1N-2N-4N ($\nu_{21}=\nu_{24}$) mechanism of divacancy migration are practically the same as those for the 1N-2N-1N mechanism (see Table IV). The anisotropy function $f(\theta,\phi)$ was defined by Eq. (4.10). Values of the relaxation rates outside the minimum regions may be obtained from Table IV. [$2a_0$ = cube edge of a unit cell; $\delta=\gamma^4\hbar^2 I(I+1)$.]

	$T_1^{-1}=[E_1+f(\theta,\phi)F_1]\,\delta a_0^{-6}\omega_0^{-1}$				$T_2^{-1}=[E_2+f(\theta,\phi)F_2]\,\delta a_0^{-6}\omega_0^{-1}$				$T_{1\rho}^{-1}=[E_3+f(\theta,\phi)F_3]\,\delta a_0^{-6}\omega_1^{-1}$			
	Single vacancies		Divacancies		Single vacancies		Divacancies		Single vacancies		Divacancies	
$\log_{10}(\omega\tau)$	E_1	F_1	E_1	F_1	E_2	F_2	E_2	F_2	E_3	F_3	E_3	F_3
−1.5	3.99×10^{-2}	-9.77×10^{-6}	7.94×10^{-2}	-8.43×10^{-5}	4.01×10^{-2}	4.95×10^{-6}	8.10×10^{-2}	4.43×10^{-5}	8.33×10^{-3}	4.50×10^{-3}	1.62×10^{-2}	9.29×10^{-3}
−1.4	4.99×10^{-2}	-1.94×10^{-5}	9.80×10^{-2}	-1.64×10^{-4}	5.04×10^{-2}	9.88×10^{-6}	1.01×10^{-1}	8.87×10^{-5}	1.04×10^{-2}	5.64×10^{-3}	1.98×10^{-2}	1.15×10^{-2}
−1.3	6.23×10^{-2}	-3.83×10^{-5}	1.20×10^{-1}	-3.16×10^{-4}	6.32×10^{-2}	1.98×10^{-5}	1.26×10^{-1}	1.78×10^{-4}	1.29×10^{-2}	7.06×10^{-3}	2.39×10^{-2}	1.42×10^{-2}
−1.2	7.73×10^{-2}	-7.52×10^{-5}	1.44×10^{-1}	-5.97×10^{-4}	7.91×10^{-2}	3.95×10^{-5}	1.56×10^{-1}	3.57×10^{-4}	1.59×10^{-2}	8.81×10^{-3}	2.82×10^{-2}	1.72×10^{-2}
−1.1	9.52×10^{-2}	-1.46×10^{-4}	1.70×10^{-1}	-1.10×10^{-3}	9.87×10^{-2}	7.92×10^{-5}	1.90×10^{-1}	7.18×10^{-4}	1.94×10^{-2}	1.09×10^{-2}	3.25×10^{-2}	2.05×10^{-2}
−1.0	1.16×10^{-1}	-2.81×10^{-4}	1.96×10^{-1}	-1.94×10^{-3}	1.23×10^{-1}	1.59×10^{-4}	2.31×10^{-1}	1.44×10^{-3}	2.33×10^{-2}	1.35×10^{-2}	3.62×10^{-2}	2.39×10^{-2}
−0.9	1.39×10^{-1}	-5.31×10^{-4}	2.20×10^{-1}	-3.29×10^{-3}	1.51×10^{-1}	3.10×10^{-4}	2.76×10^{-1}	2.85×10^{-3}	2.74×10^{-2}	1.64×10^{-2}	3.90×10^{-2}	2.69×10^{-2}
−0.8	1.63×10^{-1}	-9.75×10^{-4}	2.40×10^{-1}	-5.24×10^{-3}	1.85×10^{-1}	6.40×10^{-4}	3.24×10^{-1}	5.57×10^{-3}	3.12×10^{-2}	1.96×10^{-2}	4.06×10^{-2}	2.92×10^{-2}
−0.7	1.88×10^{-1}	-1.73×10^{-3}	2.53×10^{-1}	-7.82×10^{-3}	2.24×10^{-1}	1.28×10^{-3}	3.74×10^{-1}	1.06×10^{-2}	3.45×10^{-2}	2.30×10^{-2}	4.08×10^{-2}	3.01×10^{-2}
−0.6	2.11×10^{-1}	-2.93×10^{-3}	2.57×10^{-1}	-1.08×10^{-2}	2.67×10^{-1}	2.54×10^{-2}	4.23×10^{-1}	1.93×10^{-2}	3.71×10^{-2}	2.61×10^{-2}	3.94×10^{-2}	2.95×10^{-2}
−0.5	2.31×10^{-1}	-4.70×10^{-3}	2.51×10^{-1}	-1.37×10^{-2}	3.14×10^{-1}	4.94×10^{-2}	4.71×10^{-1}	3.37×10^{-2}	3.90×10^{-2}	2.86×10^{-2}	3.63×10^{-2}	2.76×10^{-2}
−0.4	2.46×10^{-1}	-7.10×10^{-3}	2.37×10^{-1}	-1.58×10^{-2}	3.63×10^{-1}	9.36×10^{-2}	5.16×10^{-1}	5.60×10^{-2}	3.99×10^{-2}	2.99×10^{-2}	3.20×10^{-2}	2.47×10^{-2}
−0.3	2.53×10^{-1}	-9.96×10^{-3}	2.16×10^{-1}	-1.68×10^{-2}	4.13×10^{-1}	1.71×10^{-2}	5.59×10^{-1}	8.80×10^{-2}	3.91×10^{-2}	2.98×10^{-2}	2.74×10^{-2}	2.13×10^{-2}
−0.2	2.50×10^{-1}	-1.29×10^{-2}	1.90×10^{-1}	-1.66×10^{-2}	4.62×10^{-1}	3.00×10^{-2}	6.05×10^{-1}	1.31×10^{-1}	3.66×10^{-2}	2.82×10^{-2}	2.29×10^{-2}	1.79×10^{-2}
−0.1	2.39×10^{-1}	-1.53×10^{-2}	1.63×10^{-1}	-1.54×10^{-2}	5.11×10^{-1}	5.01×10^{-2}	6.61×10^{-1}	1.87×10^{-1}	3.28×10^{-2}	2.55×10^{-2}	1.88×10^{-2}	1.47×10^{-2}
0.0	2.21×10^{-1}	-1.66×10^{-2}	1.36×10^{-1}	1.36×10^{-2}	5.59×10^{-1}	7.95×10^{-2}	7.38×10^{-1}	2.56×10^{-1}	2.85×10^{-2}	2.22×10^{-2}	1.53×10^{-2}	1.20×10^{-2}
0.1	1.97×10^{-1}	-1.67×10^{-2}	1.12×10^{-1}	-1.16×10^{-2}	6.08×10^{-1}	1.20×10^{-1}	8.44×10^{-1}	3.41×10^{-1}	2.41×10^{-2}	1.88×10^{-2}	1.23×10^{-2}	9.68×10^{-3}
0.2	1.70×10^{-1}	-1.58×10^{-2}	9.14×10^{-2}	-9.68×10^{-3}	6.66×10^{-1}	1.72×10^{-1}	9.89×10^{-1}	4.46×10^{-1}	2.00×10^{-2}	1.56×10^{-2}	9.88×10^{-3}	7.77×10^{-3}
0.3	1.44×10^{-1}	-1.41×10^{-2}	7.38×10^{-2}	-7.93×10^{-3}	7.43×10^{-1}	2.38×10^{-1}	1.18×10^{0}	5.76×10^{-1}	1.63×10^{-2}	1.27×10^{-2}	7.90×10^{-3}	6.21×10^{-3}
0.4	1.19×10^{-1}	-1.22×10^{-2}	5.92×10^{-2}	-6.42×10^{-3}	8.48×10^{-1}	3.19×10^{-1}	1.44×10^{0}	7.37×10^{-1}	1.32×10^{-2}	1.03×10^{-2}	6.30×10^{-3}	4.95×10^{-3}
0.5	9.74×10^{-2}	-1.02×10^{-2}	4.74×10^{-2}	-5.17×10^{-3}	9.92×10^{-1}	4.19×10^{-1}	1.77×10^{0}	9.38×10^{-1}	1.06×10^{-2}	8.25×10^{-3}	5.01×10^{-3}	3.94×10^{-3}
0.6	7.88×10^{-2}	-8.38×10^{-3}	3.78×10^{-2}	-4.14×10^{-3}	1.83×10^{0}	5.42×10^{-1}	2.19×10^{0}	1.19×10^{0}	8.49×10^{-3}	6.60×10^{-3}	3.99×10^{-3}	3.14×10^{-3}
0.7	6.34×10^{-2}	-6.81×10^{-3}	3.01×10^{-2}	-3.30×10^{-3}	1.44×10^{0}	6.95×10^{-1}	2.74×10^{0}	1.50×10^{0}	6.78×10^{-3}	5.27×10^{-3}	3.17×10^{-3}	2.49×10^{-3}
0.8	5.08×10^{-2}	-5.49×10^{-3}	2.39×10^{-2}	-2.63×10^{-3}	1.76×10^{0}	8.85×10^{-1}	3.42×10^{0}	1.90×10^{0}	5.40×10^{-3}	4.20×10^{-3}	2.52×10^{-3}	1.98×10^{-3}
0.9	4.05×10^{-2}	-4.40×10^{-3}	1.90×10^{-2}	-2.10×10^{-3}	2.18×10^{0}	1.12×10^{0}	4.29×10^{0}	2.39×10^{0}	4.30×10^{-3}	3.34×10^{-3}	2.00×10^{-3}	1.58×10^{-3}
1.0	3.24×10^{-2}	-3.52×10^{-3}	1.51×10^{-2}	-1.67×10^{-3}	2.72×10^{0}	1.36×10^{0}	5.39×10^{0}	2.93×10^{0}	3.42×10^{-3}	2.66×10^{-3}	1.59×10^{-3}	1.25×10^{-3}
1.1	2.58×10^{-2}	-2.80×10^{-3}	1.20×10^{-2}	-1.33×10^{-3}	3.40×10^{0}	1.72×10^{0}	6.77×10^{0}	3.69×10^{0}	2.72×10^{-3}	2.11×10^{-3}	1.27×10^{-3}	9.94×10^{-4}
1.2	2.05×10^{-2}	-2.23×10^{-3}	9.56×10^{-3}	-1.05×10^{-3}	4.27×10^{0}	2.17×10^{0}	8.52×10^{0}	4.65×10^{0}	2.16×10^{-3}	1.68×10^{-3}	1.01×10^{-3}	7.90×10^{-4}
1.3	1.63×10^{-2}	-1.78×10^{-3}	7.59×10^{-3}	-8.36×10^{-4}	5.36×10^{0}	2.74×10^{0}	1.07×10^{1}	5.85×10^{0}	1.72×10^{-3}	1.33×10^{-3}	7.98×10^{-4}	6.28×10^{-4}
1.4	1.29×10^{-2}	-1.41×10^{-3}	6.03×10^{-3}	-6.65×10^{-4}	6.73×10^{0}	3.45×10^{0}	1.35×10^{1}	7.37×10^{0}	1.36×10^{-3}	1.06×10^{-3}	6.34×10^{-4}	4.99×10^{-4}
1.5	1.03×10^{-2}	-1.12×10^{-3}	4.79×10^{-3}	-5.28×10^{-4}	8.46×10^{0}	4.34×10^{0}	1.70×10^{1}	9.27×10^{0}	1.08×10^{-3}	8.42×10^{-4}	5.03×10^{-4}	3.96×10^{-4}

TABLE VI. Diffusion via single and double vacancies in a *fcc* crystal. For further details, see Table V.

	$T_1^{-1}=[E_1+f(\theta,\phi)F_1]\,\delta a_0^{-6}\omega_0^{-1}$				$T_2^{-1}=[E_2+f(\theta,\phi)F_2]\,\delta a_0^{-6}\omega_0^{-1}$				$T_{1\rho}^{-1}=[E_3+f(\theta,\phi)F_3]\,\delta a_0^{-6}\omega_1^{-1}$			
	Single vacancies		Divacancies		Single vacancies		Divacancies		Single vacancies		Divacancies	
$\log_{10}(\omega\tau)$	E_1	F_1	E_1	F_1	E_2	F_2	E_2	F_2	E_3	F_3	E_3	F_3
−1.5	1.49×10^{-1}	-2.76×10^{-5}	3.07×10^{-1}	-2.58×10^{-4}	1.50×10^{-1}	1.40×10^{-5}	3.14×10^{-1}	1.36×10^{-4}	3.45×10^{-2}	1.28×10^{-2}	7.04×10^{-2}	2.67×10^{-2}
−1.4	1.87×10^{-1}	-5.47×10^{-5}	3.80×10^{-1}	-5.01×10^{-4}	1.89×10^{-1}	2.79×10^{-5}	3.92×10^{-1}	2.73×10^{-4}	4.31×10^{-2}	1.60×10^{-2}	8.65×10^{-2}	3.31×10^{-2}
−1.3	2.33×10^{-1}	-1.08×10^{-4}	4.65×10^{-1}	-9.59×10^{-4}	2.37×10^{-1}	5.57×10^{-5}	4.88×10^{-1}	5.47×10^{-4}	5.37×10^{-2}	2.00×10^{-2}	1.05×10^{-1}	4.07×10^{-2}
−1.2	2.90×10^{-1}	-2.12×10^{-4}	5.61×10^{-1}	-1.80×10^{-3}	2.96×10^{-1}	1.12×10^{-4}	6.04×10^{-1}	1.10×10^{-3}	6.64×10^{-2}	2.50×10^{-2}	1.25×10^{-1}	4.93×10^{-2}
−1.1	3.58×10^{-1}	-4.13×10^{-4}	6.64×10^{-1}	-3.29×10^{-3}	3.70×10^{-1}	2.23×10^{-4}	7.41×10^{-1}	2.21×10^{-3}	8.15×10^{-2}	3.10×10^{-2}	1.45×10^{-1}	5.87×10^{-2}
−1.0	4.38×10^{-1}	-7.95×10^{-4}	7.68×10^{-1}	-5.77×10^{-3}	4.61×10^{-1}	4.48×10^{-4}	9.00×10^{-1}	4.41×10^{-3}	9.85×10^{-2}	3.81×10^{-2}	1.64×10^{-1}	6.82×10^{-2}
−0.9	5.27×10^{-1}	-1.50×10^{-3}	8.64×10^{-1}	-9.67×10^{-3}	5.70×10^{-1}	9.00×10^{-4}	1.08×10^{0}	8.71×10^{-3}	1.17×10^{-1}	4.64×10^{-2}	1.78×10^{-1}	7.67×10^{-2}
−0.8	6.24×10^{-1}	-2.76×10^{-3}	9.43×10^{-1}	-1.53×10^{-2}	6.99×10^{-1}	1.81×10^{-3}	1.27×10^{0}	1.69×10^{-2}	1.36×10^{-1}	5.56×10^{-2}	1.88×10^{-1}	8.28×10^{-2}
−0.7	7.22×10^{-1}	-4.89×10^{-3}	9.98×10^{-1}	-2.27×10^{-2}	8.48×10^{-1}	3.62×10^{-3}	1.48×10^{0}	3.18×10^{-2}	1.53×10^{-1}	6.51×10^{-2}	1.91×10^{-1}	8.52×10^{-2}
−0.6	8.16×10^{-1}	-8.30×10^{-3}	1.02×10^{0}	-3.11×10^{-2}	1.02×10^{0}	7.16×10^{-3}	1.68×10^{0}	5.76×10^{-2}	1.67×10^{-1}	7.40×10^{-2}	1.86×10^{-1}	8.33×10^{-2}
−0.5	9.00×10^{-1}	-1.34×10^{-2}	9.95×10^{-1}	-3.91×10^{-2}	1.20×10^{0}	1.40×10^{-2}	1.88×10^{0}	1.00×10^{-1}	1.79×10^{-1}	8.10×10^{-2}	1.72×10^{-1}	7.75×10^{-2}
−0.4	9.66×10^{-1}	-2.02×10^{-2}	9.38×10^{-1}	-4.50×10^{-2}	1.40×10^{0}	2.65×10^{-2}	2.07×10^{0}	1.65×10^{-1}	1.86×10^{-1}	8.47×10^{-2}	1.53×10^{-1}	6.92×10^{-2}
−0.3	1.00×10^{0}	-2.83×10^{-2}	8.55×10^{-1}	-4.76×10^{-2}	1.60×10^{0}	4.84×10^{-2}	2.27×10^{0}	2.58×10^{-1}	1.86×10^{-1}	8.42×10^{-2}	1.32×10^{-1}	5.96×10^{-2}
−0.2	9.95×10^{-1}	-3.65×10^{-2}	7.54×10^{-1}	-4.67×10^{-2}	1.81×10^{0}	8.50×10^{-2}	2.48×10^{0}	3.82×10^{-1}	1.77×10^{-1}	7.97×10^{-2}	1.11×10^{-1}	5.01×10^{-2}
−0.1	9.56×10^{-1}	-4.32×10^{-2}	6.46×10^{-1}	-4.32×10^{-2}	2.01×10^{0}	1.42×10^{-1}	2.75×10^{0}	5.42×10^{-1}	1.61×10^{-1}	7.21×10^{-2}	9.12×10^{-2}	4.13×10^{-2}
0.0	8.86×10^{-1}	-4.69×10^{-2}	5.41×10^{-1}	-3.82×10^{-2}	2.22×10^{0}	2.26×10^{-1}	3.10×10^{0}	7.41×10^{-1}	1.41×10^{-1}	6.28×10^{-2}	7.42×10^{-2}	3.36×10^{-2}
0.1	7.93×10^{-1}	-4.72×10^{-2}	4.46×10^{-1}	-3.26×10^{-2}	2.44×10^{0}	3.40×10^{-1}	3.57×10^{0}	9.87×10^{-1}	1.20×10^{-1}	5.32×10^{-2}	5.99×10^{-2}	2.71×10^{-2}
0.2	6.89×10^{-1}	-4.46×10^{-2}	3.63×10^{-1}	-2.71×10^{-2}	2.69×10^{0}	4.88×10^{-1}	4.22×10^{0}	1.29×10^{0}	1.00×10^{-1}	4.41×10^{-2}	4.81×10^{-2}	2.17×10^{-2}
0.3	5.84×10^{-1}	-3.99×10^{-2}	2.93×10^{-1}	-2.22×10^{-2}	3.02×10^{0}	6.74×10^{-1}	5.07×10^{0}	1.66×10^{0}	8.22×10^{-2}	3.60×10^{-2}	3.84×10^{-2}	1.74×10^{-2}
0.4	4.85×10^{-1}	-3.44×10^{-2}	2.35×10^{-1}	-1.80×10^{-2}	3.47×10^{0}	9.04×10^{-1}	6.19×10^{0}	2.13×10^{0}	6.67×10^{-2}	2.91×10^{-2}	3.07×10^{-2}	1.39×10^{-2}
0.5	3.97×10^{-1}	-2.89×10^{-2}	1.88×10^{-1}	-1.45×10^{-2}	4.07×10^{0}	1.19×10^{0}	7.63×10^{0}	2.71×10^{0}	5.37×10^{-2}	2.34×10^{-2}	2.44×10^{-2}	1.10×10^{-2}
0.6	3.22×10^{-1}	-2.38×10^{-2}	1.50×10^{-1}	-1.16×10^{-2}	4.87×10^{0}	1.54×10^{0}	9.48×10^{0}	3.43×10^{0}	4.30×10^{-2}	1.87×10^{-2}	1.94×10^{-2}	8.78×10^{-3}
0.7	2.59×10^{-1}	-1.93×10^{-2}	1.20×10^{-1}	-9.24×10^{-3}	5.91×10^{0}	1.97×10^{0}	1.18×10^{1}	4.33×10^{0}	3.43×10^{-2}	1.49×10^{-2}	1.54×10^{-2}	6.98×10^{-3}
0.8	2.08×10^{-1}	-1.56×10^{-2}	9.52×10^{-2}	-7.37×10^{-3}	7.27×10^{0}	2.51×10^{0}	1.48×10^{1}	5.47×10^{0}	2.74×10^{-2}	1.19×10^{-2}	1.23×10^{-2}	5.55×10^{-3}
0.9	1.66×10^{-1}	-1.25×10^{-2}	7.57×10^{-2}	-5.86×10^{-3}	9.01×10^{0}	3.18×10^{0}	1.86×10^{1}	6.90×10^{0}	2.18×10^{-2}	9.48×10^{-3}	9.75×10^{-3}	4.41×10^{-3}
1.0	1.33×10^{-1}	-9.98×10^{-3}	6.02×10^{-2}	-4.67×10^{-3}	1.12×10^{1}	4.03×10^{0}	2.33×10^{1}	8.69×10^{0}	1.74×10^{-2}	7.54×10^{-3}	7.75×10^{-3}	3.50×10^{-3}
1.1	1.05×10^{-1}	-7.96×10^{-3}	4.78×10^{-2}	-3.71×10^{-3}	1.41×10^{1}	5.08×10^{0}	2.94×10^{1}	1.10×10^{1}	1.38×10^{-2}	5.99×10^{-3}	6.16×10^{-3}	2.78×10^{-3}
1.2	8.37×10^{-2}	-6.33×10^{-3}	3.80×10^{-2}	-2.95×10^{-3}	1.76×10^{1}	6.41×10^{0}	3.69×10^{1}	1.38×10^{1}	1.10×10^{-2}	4.76×10^{-3}	4.89×10^{-3}	2.21×10^{-3}
1.3	6.66×10^{-2}	-5.04×10^{-3}	3.02×10^{-3}	-2.34×10^{-3}	2.21×10^{1}	8.08×10^{0}	4.64×10^{1}	1.74×10^{1}	8.70×10^{-3}	3.78×10^{-3}	3.89×10^{-3}	1.76×10^{-3}
1.4	5.29×10^{-2}	-4.00×10^{-3}	2.40×10^{-2}	-1.86×10^{-3}	2.78×10^{1}	1.02×10^{1}	5.85×10^{1}	2.19×10^{1}	6.91×10^{-3}	3.01×10^{-3}	3.09×10^{-3}	1.40×10^{-3}
1.5	4.20×10^{-2}	-3.18×10^{-3}	1.91×10^{-2}	-1.48×10^{-3}	3.50×10^{1}	1.28×10^{1}	7.36×10^{1}	2.75×10^{1}	5.49×10^{-3}	2.39×10^{-3}	2.45×10^{-3}	1.10×10^{-3}

TABLE VII. Geometrical factors g_1, g_2 (in units of the nearest-neighbor distance d) and $g_{12}=g_1/g_2$ for the vacancy mechanisms considered in this paper as presented by Mehrer (Ref. 3). Interestingly, for the 1N-2N-4N mechanism g_2 and, therefore, g_{12} is independent of the ratio ν_{21}/ν_{24}.

	g_1 (monovacancies)	g_2 (divacancies) 1N-2N-1N	g_2 (divacancies) 1N-2N-4N	$g_{12}=g_1/g_2$
bcc	1	2	2	$\frac{1}{2}$
fcc	1	$\frac{2}{3}$	...	$\frac{3}{2}$

calculation of the corresponding value of $\log_{10}(\omega\tau)$.

(ii) For every value of E_1/kT, $p_1(T)$ and $p_2(T)$ may be determined from Eq. (4.8) and the normalization condition $p_1(T)+p_2(T)=1$, using the values of $g_{\alpha\beta}$ listed in Table VII.

(iii) Finally, the values of the relaxation rates at that temperature are obtained from Eq. (5.3) and the results for $(T_{\rm rel}^{-1})_\alpha$ ($\alpha=1,2$) in Fig. 5, or from the appropriate interpolation between the values listed in Tables V and VI, respectively.

Following this procedure, Figs. 6 and 7 have been obtained. Also shown there is the increase of the probability p_2 that atomic jumps are due to divacancies and not single vacancies. According to Fig. 6, for $\epsilon=0.20$ and $D_{21}=30$, p_2 increases from 10% to 73% in the temperature range chosen. For $D_{21}=100$ these values become 27% and 90%, respectively. Similarly, choosing $\epsilon=0.30$, p_2 increases from 1% to 52% for $D_{21}=30$, and from 3% to 79% for $D_{21}=100$ (see Fig. 7) for our choice of ω_0 and ω_1, respectively.

The first term on the right-hand side of Eq. (5.2) is temperature independent. For a given value of ω_0 or ω_1, respectively, the magnitude of this term governs the *position* of the T_1 or $T_{1\rho}$ minimum with respect to the temperature region where the dominant diffusion mechanism changes. For the plots shown in Figs. 6 and 7, this term was chosen to be 10^{-7} ($\omega_0=2\pi\nu_0\approx 10^8$ sec^{-1}; $d^2\approx 6\times10^{-16}$ cm^2; $D_{01}\approx 0.1$ cm^2 sec^{-1}).

For the hypothetical change of diffusion mechanism from divacancies assumed to dominate at *low* temperatures (E_1 is then identified with the activation energy for divacancies) to single vacancies at *higher* temperatures, the curves shown in Fig. 8 are expected.

This case, in fact not realistic at all, shows a general feature of the method suggested here: the shape and width of the T_1 and $T_{1\rho}$ minima as a function of inverse temperature differ significantly for the hypothetical change of the dominant diffusion mechanism from one mechanism to another and for the reverse transition. These differences are the greater the more the *absolute values* of the relaxation times at a given temperature differ for the individual diffusion mechanisms (see, e.g., Fig. 5.), i.e., the more the numbers of relative jumps of some spin pair i-m vary from one mechanism to another (see also Sec. III A and Table I).

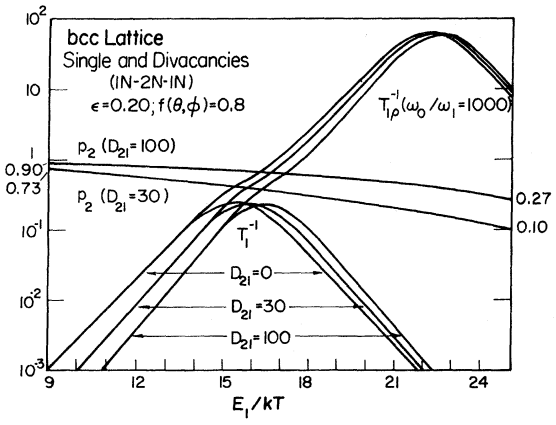

FIG. 6. Relaxation rates and probabilities p_2 as a function of E_1/kT and the parameters ϵ and D_{21} for mono- and divacancies (1N − 2N − 1N) in a powdered [$f(\theta,\phi)=0.8$] bcc sample for $D_{21}=30.0$ and 100.0, respectively, and $\epsilon=0.20$. Up to a few percent the plots are the same for a 1N-2N-4N mechanism. (Units as in Fig. 3).

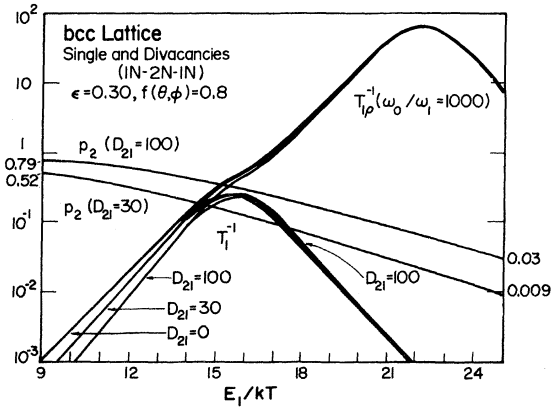

FIG. 7. All parameters are identical with those chosen in Fig. 6 except $\epsilon=0.30$.

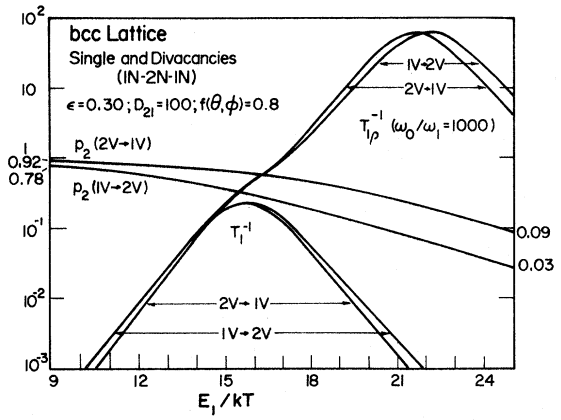

FIG. 8. Curves named $1V \rightarrow 2V$ (identical with the corresponding plot in Fig. 7 for $\epsilon = 0.30$, $D_{21} = 100$) represent the relaxation rates T_1^{-1} and $T_{1\rho}^{-1}$ for the temperature-dependent admixture of divacancies (1N-2N-1N) to monovacancies in a bcc lattice [$f(\theta, \phi) = 0.8$]. Second set of curves, labeled $2V \rightarrow 1V$, would be expected for the hypothetic change of diffusion mechanism from divacancies at low temperature (with activation energy E_1), to single vacancies at higher temperatures. Owing to the differences between g_{12} and g_{21} [see Table VII and Eq. (4.8)], $p_2(E_1/kT)$ is a different function for the two cases. (Units as in Fig. 3.)

VI. ON THE DETERMINATION OF SELF-DIFFUSION MECHANISMS BY NMR

As illustrated in Secs. V B and V C and in Ref. 11b, in terms of the anisotropies of T_1, T_2, and $T_{1\rho}$ (in the high-field limit) there is little chance ever to identify different defect mechanisms of self-diffusion. (The effect of two diffusion mechanisms on the anisotropy of $T_{1\rho}$ in the so-called Slichter-Ailion region will be discussed elsewhere.) However, as illustrated above, the *shapes* of the T_1 and $T_{1\rho}$ minima as a function of temperature are strongly influenced by a temperature-dependent admixture of a second diffusion mechanism to the mechanism dominant at low temperatures. Since in both single crystals and powdered samples the features of these minima characterize both diffusion mechanisms involved, a new method to study the mechanisms of self-diffusion in metals and ionic crystals is thus proposed.

A. Detection of the admixture of divacancies to the dominant monovacancy mechanism in metals

Figures 6–8 suggest the following procedure to detect an admixture of divacancies to the monovacancies usually dominant at lower temperatures ($T < \frac{2}{3} T_m$):

(i) Assuming that on the low-temperature side of the $T_{1\rho}$ minimum single vacancies represent the dominant diffusion mechanism, the parameters E_1 and D_{01} may be determined by analyzing the related $T_{1\rho}$ values in this region.

(ii) In favorable cases, in the temperature region where the dominant diffusion mechanism changes (and where, therefore, the corresponding Arrhenius plot shows a curvature), both the T_1 and the $T_{1\rho}$ minimum are experimentally accessible. From a computer fit of the theoretical predictions for T_1 and $T_{1\rho}$ [see Tables V and VI and Eqs. (5.3) and (4.8)], the adjustable parameters ϵ and D_{21} may be determined.

(iii) Using the values of the parameters E_1, D_{01}, ϵ, and D_{21} thus obtained, values of the self-diffusion coefficient D as a function of temperature may be calculated from Eqs. (4.7) and (1.3) thus allowing the comparison of NMR relaxation data with diffusion coefficients measured by other (usually more direct) experimental techniques.

In essence following this outline, an attempt to determine the four parameters E_1, D_{01}, ϵ, and D_{21} was recently made by Messer and Noack[22] who analyzed both T_1 and $T_{1\rho}$ minima in lithium metal for several values of both the large Zeeman field H_0 and the rotating field H_1. However, owing to the uncertainties inherent in the simplified theory of Cavelius[13,14] (see also Sec. I), the agreement of Messer and Noack's data with the theory is not too good. Their investigations, nevertheless, seem to indicate a narrowing of the T_1 minimum when shifted towards higher temperatures by increasing the Larmor frequency ω_0, an effect also predicted in this article (see, e.g., Figs. 6 and 7). A reinterpretation of these experiments in terms of the above theory is therefore desirable.

B. Analysis of self-diffusion in ionic crystals

Owing to the requirement of charge neutrality, the doping with impurities of different valency than the host atoms allows to influence the equilibrium concentrations of defects in ionic crystals. The values of D_{01} and E_1 in the temperature region where *extrinsic* diffusion dominates are usually very different from D_{02} and E_2 characterizing the *intrinsic* diffusion mechanism. If it is possible (e.g., by appropriate doping concentrations or by the choice of ω_0 or ω_1) to measure the $T_{1\rho}$ or T_1 minima in the rather narrow region where the transition from extrinsic to intrinsic diffusion occurs, the analysis of the relaxation minima in terms of the transition, e.g., from interstitialcy to vacancy-induced self-diffusion and vice versa, may allow one to identify *both* diffusion mechanisms involved.

Note added in proof. The case in which the curvature of the Arrhenius plot is fully attributed to the temperature dependence of D_{01} and E_1 is discussed in a forthcoming article by this author in the Proceedings of the International Conference on Atomic Defects in Metals, Argonne 1976 (unpublished).

ACKNOWLEDGMENTS

I am indebted to Professor A. Seeger for his stimulating interest and encouragement. Discussions with Dipl. Phys. S. Dais on some aspects of this article were very helpful. David Steck's assistance with some of the computer calculations is gratefully acknowledged.

---

*Research on this subject was initiated during my appointment at the Max-Planck-Institut für Metallforschung, Institut für Physik, Stuttgart, West Germany.

[1]See, e.g., A. Seeger, J. Less-Common Metals 28, 387 (1972); A. Seeger and H. Mehrer, in *Vacancies and Interstitials in Metals,* edited by A. Seeger, D. Schumacher, W. Schilling, and J. Diehl (North-Holland, Amsterdam, 1970).

[2]H. Mehrer and A. Seeger, Cryst. Lattice Defects 3, 1 (1972).

[3]H. Mehrer, Habilitationsschrift (Universität Stuttgart, 1973) (unpublished).

[4]R. J. Lysiak and P. P. Mahendroo, Phys. Rev. 44, 4025 (1966).

[5]R. W. Ure, Phys. Rev. 26, 1363 (1957).

[6]W. Bollmann, P. Görlich, W. Hauk, and H. Mothes, Phys. Status Solidi A 2, 157 (1970).

[7]M. Eisenstadt and A. G. Redfield, Phys. Rev. 132, 635 (1963).

[8]D. Wolf, Phys. Rev. B 10, 2710 (1974).

[9]D. C. Ailion and P. P. Ho, Phys. Rev. 168, 662 (1968).

[10]D. Wolf, Phys. Rev. B 10, 2724 (1974).

[11](a) D. Wolf, *Proceedings of the Eighteenth Ampère Congress, Nottingham, 1974* (Nottingham University Press, Nottingham, England, 1975), p. 251; (b) D. Wolf, D. R. Figueroa and J. Strange, Phys. Rev. B (to be published).

[12]A. Abragam, *The Principles of Nuclear Magnetism* (Clarendon, Oxford, 1961), Chap. VIII.

[13]E. Cavelius, Phys. Status Solidi B 95, 181 (1974).

[14]D. Wolf, Z. Naturforsch. A 26, 1816 (1971).

[15]H. C. Torrey, Phys. Rev. 92, 962 (1953).

[16]D. Wolf, J. Magn. Res. 17, 1 (1975).

[17]C. A. Sholl, J. Phys. C. 7, 3378 (1975).

[18]D. C. Look and I. J. Lowe, J. Chem. Phys. 44, 2995 (1966).

[19]D. Wolf and P. Jung, Phys. Rev. B 12, 3596 (1975).

[20]H. Mehrer, J. Phys. F 3, 543 (1973).

[21]D. Wolf and K. Differt, Comput. Phys. Commun. (to be published).

[22]R. Messer and F. Noack, Appl. Phys. 6, 79 (1975).